Applied Thermal Engineering 212 (2022) 118635

Contents lists available at ScienceDirect

Applied Thermal Engineering

journal homepage: www.elsevier.com/locate/apthermeng

Research Paper

Experimental investigation on the performance of a novel thermo-mechanical refrigeration system driven by an expander-compressor unit

Ahmad K. Sleiti *, Wahib A. Al-Ammari, Mohammed Al-Khawaja, Ahmad T. Saker

Department of Mechanical & Industrial Engineering, College of Engineering, Qatar University, Doha, Qatar

ARTICLE INFO

Keywords:
Thermo-mechanical refrigeration
Experimental investigation
Expander-compressor unit
COP
Evaporation capacity
R134a

ABSTRACT

Operating thermos-mechanical refrigeration (TMR) ejector-based and organic Rankine cycle-based refrigeration systems at ultra-low temperature heat source (60 °C to 100 °C) is challenging and limited by their low coefficient of performance (COP), instability, and high cost. To overcome these limitations, an innovative TMR system consists of a power loop coupled with a cooling loop through an expander-compressor unit (ECU) was introduced. To ensure the efficient operation, reliability, and flexibility, of the ECU-based TMR system, a thorough experimental investigation is presented in this study. In the present setup, an air compressor is used to provide pressurized air to drive the ECU at a desired pressure of 620 kPa. Using R134a as a refrigerant, the performance of the ECU-based refrigeration system is systematically tested for various operating conditions including refrigerant mass, evaporator pressure, temperature and flow rate of the water used for evaporation and condensation loads. All tests are performed at two operating frequencies of the ECU (0.50 Hz and 0.33 Hz). Over a wide range of testing conditions, the results show that the average COP Hz varies from 1.57 to 2.73 at 0.50 Hz and from 1.56 to 2.39 at 0.33 Hz. Moreover, the evaporator temperature reaches less than −10 °C at 0.50 Hz and −9.60 °C at 0.33 Hz. These experimental results prove that the COP of the ECU-based refrigeration system is three times higher than the ejector-based systems and 2.70 times higher than the organic Rankine cycle-based systems.

1. Introduction

Air conditioning and refrigeration systems in residential, industrial, and commercial applications consume up to 10% of the global energy production [1] and this consumption is projected to increase continuously. Without improving the energy efficiency of these systems and introducing innovative alternatives that utilize various energy sources to produce cooling effect, the energy demand for the cooling systems will be tripled by 2050 [1]. This increases the greenhouse gas emissions, which aggravates the risks of global warming and ozone depletion problems [2]. Therefore, researchers around the world devote significant efforts to replace the conventional electric-based cooling systems with other thermal energy-based or renewable energy-based cooling systems [3,4].

In literature, the thermal energy-based systems categorized according to their operating mechanism into thermos-chemical refrigeration (TCR) systems [5] and thermo-mechanical refrigeration (TMR) systems [6]. On one hand, TCR systems include closed-sorption and open-sorption processes, which have complex configurations, limitations on the evaporator and generator temperatures, and a low coefficient of performance (COP) [7]. On the other-hand, TMR systems mainly include ORC-based, and Ejector-based systems. The ejector-based systems suffer from the instability of the ejector operation with the variation of the operating conditions and have low COP [8,9]. The ORC-based systems are expensive and have limitations on the temperatures of the heat sources [10,11]. Therefore, to overcome these limitations, Sleiti et al [12] have developed an efficient, simple, flexible, and reliable thermo-mechanical refrigeration (TMR) system that directly converts the thermal energy with ultra-low temperature source into mechanical energy to compress the refrigerant of the cooling cycle using an expander-compressor unit (ECU). While, there are numerous theoretical studies that investigate the performance and applications of the ORC-based [13,14] and Ejector based systems [15,16], only four studies were introduced for the ECU-based TMR system as briefly summarized in the next paragraph.

* Corresponding author.
E-mail address: asleiti@qu.edu.qa (A.K. Sleiti).

https://doi.org/10.1016/j.applthermaleng.2022.118635
Received 15 January 2022; Received in revised form 4 April 2022; Accepted 5 May 2022
Available online 10 May 2022

Nomenclature

Symbol	Description Units
A	Cross-sectional/surface area m^2
D	Piston diameter mm
h	Specific enthalpy at specified state. kJ/kg
L	Piston stroke length. mm
$\dot{m}_R$	Mass flow rate of the refrigerant.kg/s
N	Frequency of the expander-compressor unit (ECU). Hz
P	Pressure at a specified location kPa
Q	Heat transfer rate kW
T	Temperature at a specified location ^oC
v	Specific volume of the working fluid at a specified state m^3/kg
$\dot{W}$	Power consumed by the compression process. kW

Subscripts

amb	Of the ambient air
avg	average
co	Of the condenser
Cold	Of the cold water
c,in & c,out	At the inlet and outlet of the cold water, respectively
comp.	Of the compressor
ECU	For the expander-compressor unit
ev	Of the evaporator
hot	Of the hot water
h,in & h,out	At the inlet and outlet of the hot water, respectively
in	At the inlet
out	At the outlet

Abbreviations

COP	Coefficient of performance.
ECU	Expander-compressor unit.
ORC	Organic Rankine cycle.
TCR	Thermo-chemical refrigeration systems
TMR	Thermo-mechanical refrigeration system.

In 2020, Sleiti et al. [12] conducted a comprehensive review on the various refrigeration systems with a focus on the innovative approaches of the TMR systems. They highlighted the features and limitations of the electric-based and heat-driven-based cooling system. Also, they introduced a new approach to developing an isobaric engine (based on the work developed by Encontech BV [17]) to drive a vapor-compression refrigeration cycle using waste heat sources (as an energy source) even with ultra-low temperature sources (~70 °C). The new system integrates a power loop (that generates pressurized vapor of working fluid) with a cooling loop using an expander-compressor unit (ECU). Then, Sleiti et al. [18] theoretically investigated the performance of a TMR system using an ECU powered by low-grade heat with a temperature range of (60 °C to 100 °C) at a design cooling capacity of 1 kW and evaporation temperatures of −10 °C to 5 °C. They concluded that the COP of the ECU-based cooling cycle varies between 1.2 and 2.6, which is significantly higher than those of the other thermo-mechanical refrigeration systems such as absorption-based (COP: 0.3 – 0.7) and ejector-based systems (COP: 0.1 – 0.62). Further improvement for the ECU-based cooling system is proposed by Sleiti et al. [19] via implementing a regeneration process through the power loop of the ECU-based refrigeration system. However, they found that the regeneration process improves the efficiency of the power loop only by 1%. After that, Sleiti [20] developed a database for the most suitable working fluids for various types of isobaric engines over a wide range of heat source temperatures (40 °C to 400 °C). He reported that ammonia and R32 show the highest power loop efficiencies (11%) at high pressure of 50 bar for the temperature range of 100–300 °C. Also, the refrigerant R161 has high performance for pressures between 10 and 50 bar for the full range of temperatures from 80 to 300 °C, which makes R161 the choice fluid for a wide range of applications. To investigate the performance of the ECU-based refrigeration system at high cooling capacity (>100 kW), Al-Khawaja et al. [21] investigated the performance of several parallel-connected ECUs driven by the available heat from abandoned oil wells to support district cooling network. They concluded that at a geothermal

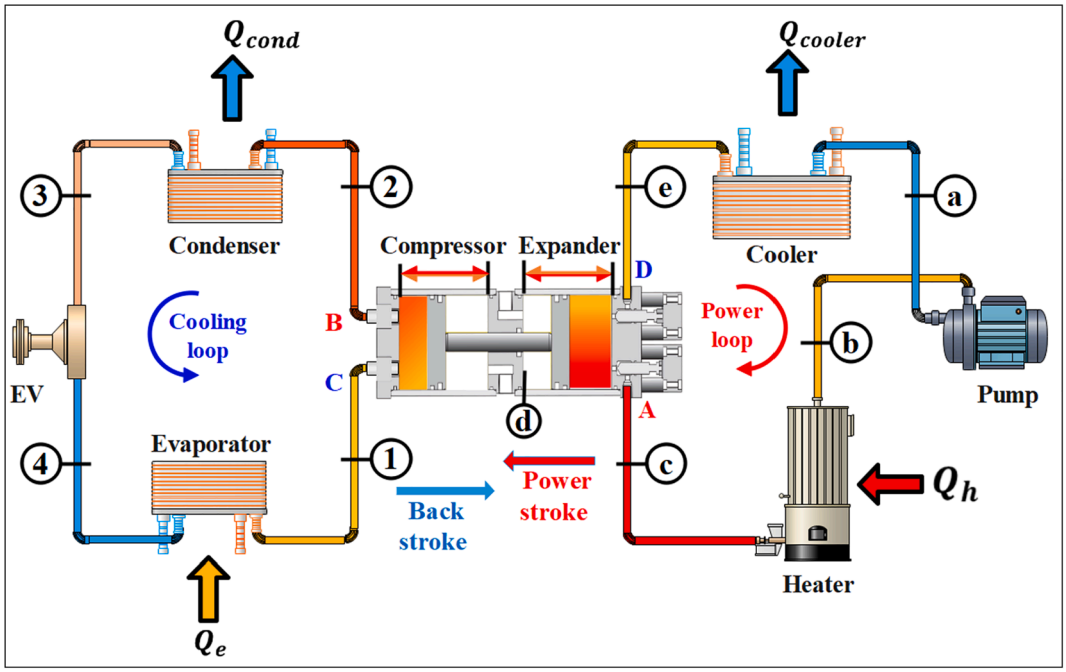

Fig. 1. Configuration of the ECU-based refrigeration system.

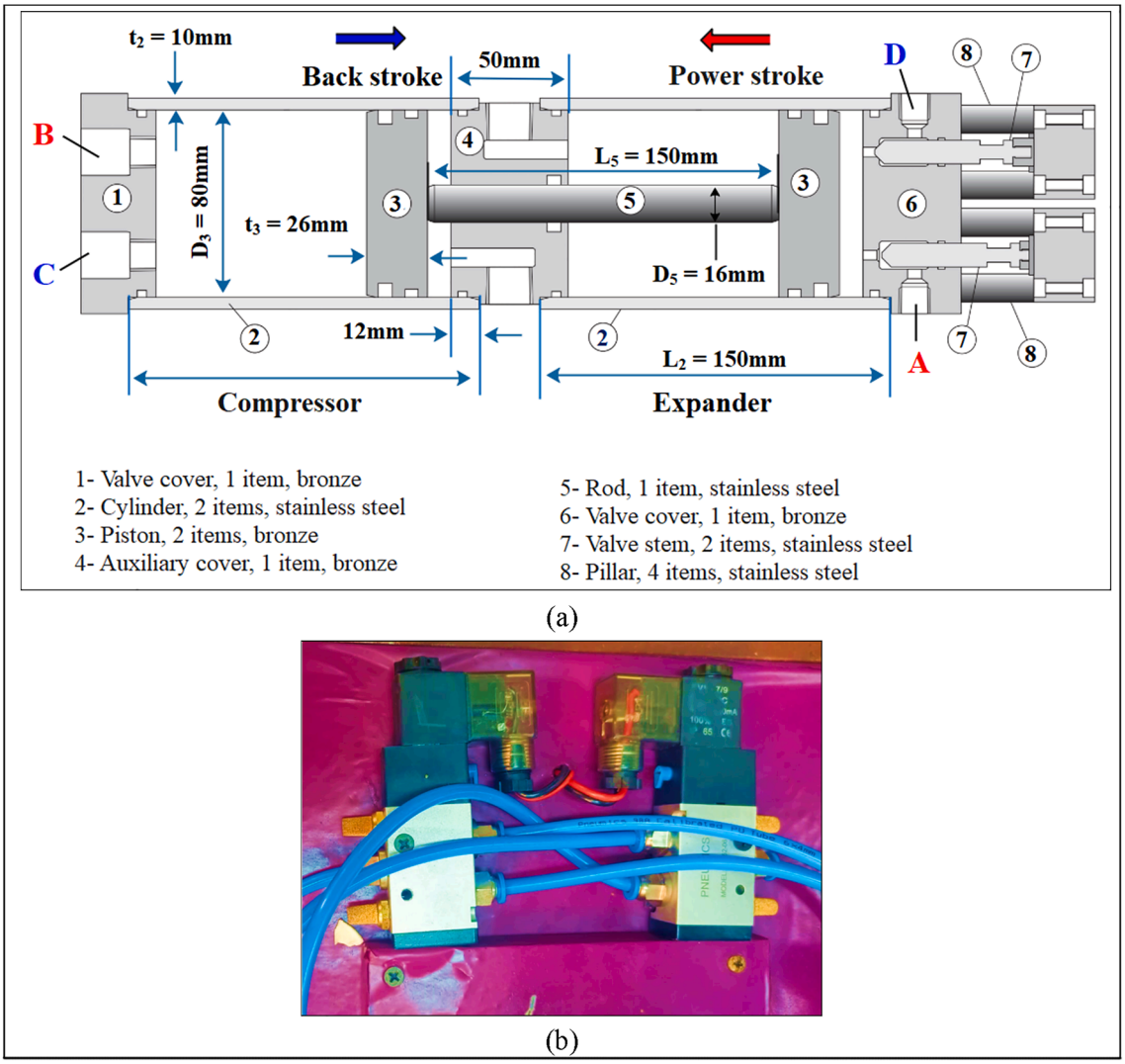

Fig. 2. Detailed design of (a) the expander-compressor unit (ECU), and (b) pneumatic solenoid valves.

temperature of 150 °C, soil temperature of 29 °C, and with R1234ze(E) as the working fluid, a cooling load of 100 kW could be generated using 20 units of ECUs.

In addition to the theoretical studies, experimental-based works are needed as a fundamental step to characterize the actual performance of the TMR systems. However, only few studies that experimentally investigated the performance of the ORC-based and Ejector-based systems were conducted. In 2017, Jiang et al. [22] experimentally tested an ORC-based cooling system integrated with a sorption system using R245fa at a heat source temperature of 75 °C to 95 °C and evaporation temperature of 10 °C. They reported that the COP varies from 1.61 to 1.90. Another experimental work for ORC-based integrated with sorption system is introduced by Chaiyat et al. [23]. They used R245fa with a heat source temperature of 105 °C and evaporation temperature of 8 °C with a COP that varies between 0.52 and 0.60. For ejector-based systems, several experimental studies were conducted at cooling capacity less than 1 kW as reviewed by Zeyghami et al. [6]. Recently, Huang et al. [24] conducted an experimental and modeling investigation on thermally-driven subcritical and transcritical ejector refrigeration systems using refrigerant R32 as the working fluid. Their system is tested at a generator temperature of 88 °C to 126 °C with a COP varied between 0.25 and 0.60. Other experimental investigations have been conducted on the performance and improvements of certain components (such as a double-slider adjustable ejector [25], ejector-expansion freezer [26], ejector geometry [27], and ORC scroll expander [28]) rather than the analysis of the overall performance of the system.

From these above-mentioned studies, it can be concluded that the ECU-based refrigeration system has several features over the other TMR systems including higher COP, wide range of applications (from low to large scale of cooling capacities), simplicity, practicable with several refrigerants, and efficient working with low-grade temperature heat sources. As it is a new innovative system, the ECU-based refrigeration cycle lacks experimental tests to prove the mentioned features. Therefore, in the present work, experimental tests are systematically conducted to examine the performance of the ECU-based refrigeration system. The ECU is fabricated and installed with a refrigeration cycle that is designed for an evaporation capacity of 0.50 kW using R134a as a refrigerant. The pressurized working fluid vapor (which is theoretically generated by the power loop driven by a low-grade heat source) is replaced with an air compressor that provides compressed air at 620 kPa. Further details about the theoretical ECU-based refrigeration system and its experimental setup are provided in Section 2 and Section 3. The methodology of the thermodynamic analysis, testing procedures, validation, and experimental uncertainty analysis are presented in Section 4. In Section 5, the results of the systematic experimental tests for the effects of various operating conditions on the performance indicators of the ECU-based refrigeration system are presented and discussed. Finally, the main findings of the present work are summarized in

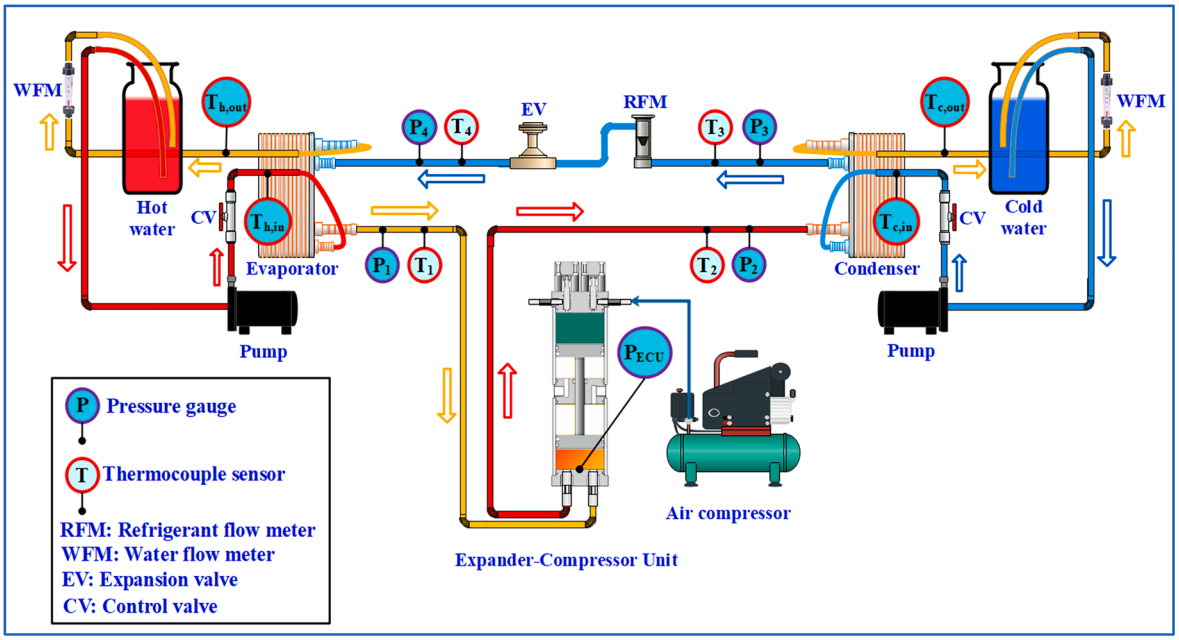

Fig. 3. Schematic diagram of the experimental layout with an air compressor plays the role of the power loop.

Section 6.

2. Background of the theoretical ECU-based refrigeration system

The theoretical configuration of the ECU-based refrigeration system is presented in Fig. 1. It consists of two loops: a power loop and a cooling loop. The power loop is composed of a pump, heater, expander cylinder, and cooler. The cooling loop is composed of the evaporator, compressor cylinder, condenser, and expansion valve. The main function of the power loop is to provide pressurized vapor of a selected fluid to perform an expansion process in the expander cylinder of the ECU. This is performed by first pumping the working fluid (i.e. R134a) of the power loop from the low-pressure side (state a) at the liquid phase to the high-pressure side (state b). Then, the pressurized fluid is directed to the heater to be heated up to saturated or super-heated vapor (state c) using an ultra-low heat source with a minimum temperature of 70 °C. Next, the pressurized vapor is expanded through the expander cylinder (process c-d) to compress the refrigerant (i.e R134a) of the cooling loop from the evaporator pressure (state 1) to the condenser pressure (state 2). The expansion of the power loop fluid to compress the refrigerant of the

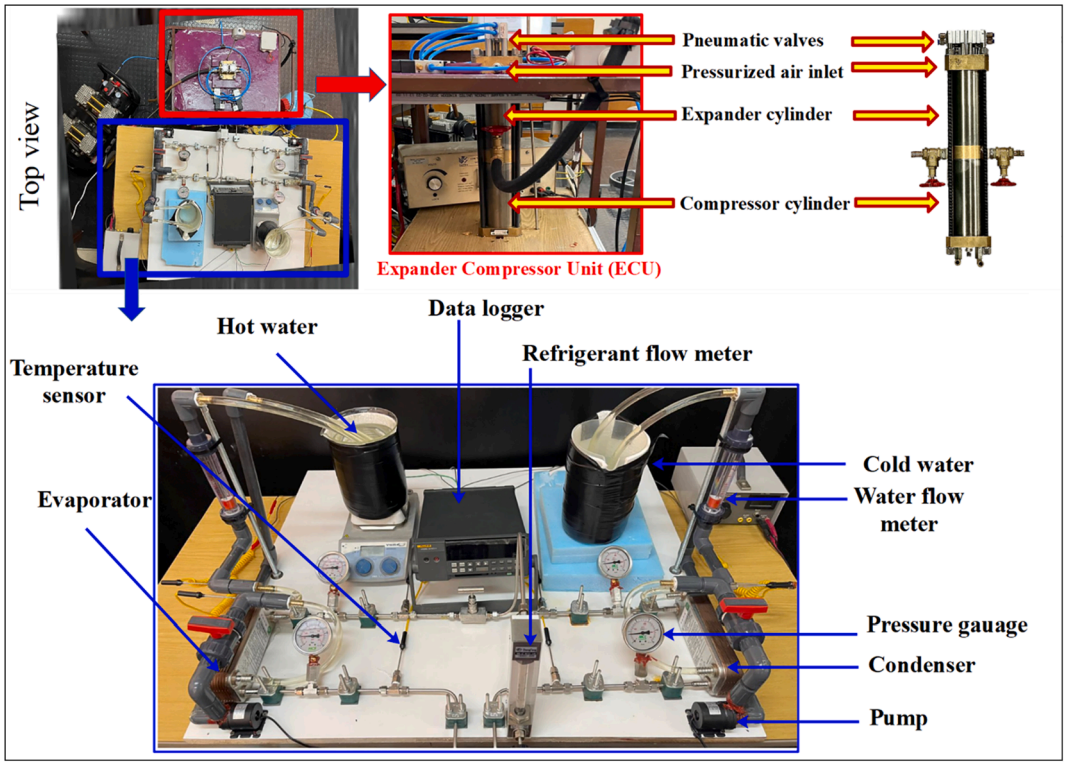

Fig. 4. Experimental setup.

cooling loop is referred to as “Power stroke”. During the power stroke, valves A and B are opened, and valves C and D are closed. The compressed refrigerant is condensed through the condenser (2–3), expanded through the expansion valve (3–4), and evaporated by the cooling load of the evaporator (4–1) and leave the evaporator at saturated or superheated refrigerant. At this instant, valves A and B are closed, and valves C and D are opened to return the pistons of the expander and compressor chambers to their original position with the help of the evaporator pressure and the venting of the power loop fluid vapor to the cooler. This process is called “Back-stroke”. Then, the working fluid of the power loop is cooled in the cooler to its initial state at the inlet of the pump (e-a) to repeat the cycle.

Therefore, the power loop converts the thermal energy provided using a heater to mechanical work to compress the refrigerant using the ECU unit shown in Fig. 2(a). It consists of two chambers (expander and compressor chambers, items # 2) with a piston in each chamber. The expander and compressor pistons are connected (item # 3) with a rigid rod (item # 5). The diameters of each piston (80 mm) and the length of the stroke (100 mm) are fabricated for a designed cooling capacity of 0.50 kW at expander pressure from 200 kPa to 800 kPa [18]. To perform the power stroke and back-stroke in continuous alternation, the valves of the expander chambers (A and D) must be forced controlled to adjust their opening and closing times. This is possible using electric, hydraulic, or pneumatic actuators. In the present experimental work, pneumatic solenoid valves are used as shown in Fig. 2(b). In contrast, the valves of the compressor cylinder are self-actuating non-return valves. To prevent the leakage of the working fluids in each cylinder, each piston was sealed using ethylene-propylene O-rings (EPDM 72x80x4). These O-rings have excellent ozone and chemical resistance properties and are compatible with many polar fluids that adversely affect other elastomers. The ports of the auxiliary cover of the ECU (item 4 in Fig. 2(a).) are used for the lubrication process of the ECU pistons using a refrigeration oil. The lubricant oil (Suniso SL32) creates a seal between the piston rings and cylinder wall, which reduces wear, provides better compression. Also, the lubricant oil provides stability and corrosion protection which extends service life and minimizes maintenance costs.

3. Experimental setup description

As mentioned above, the function of the power loop is to provide pressurized vapor of its working fluid at a suitable pressure to drive the ECU. From the theoretical analysis of the ECU-based TMR system by Sleiti et al. [18], three fluids were recommended as working fluid for the power loop, which are R717, R1234yf, and R1234ze. Furthermore, the high-pressure of the power loop was changed from 200 kPa to 800 kPa for cooling capacity of 0.50 kW. Therefore, to provide that pressure, and to maintain compact size for the experiment setup, an air compressor is used to drive the ECU as shown in Fig. 3 at supply pressure of 620 kPa. Moreover, as the compressed air has lower density and higher viscosity than the recommended refrigerants under the same conditions, its utilization forms harsh environment for the ECU test and guarantee its efficient operation with compressed refrigerants at ultra-low temperature (70 °C–100 °C).

The air compressor model is ZB-0.12/8 with a rated power of 2.24 kW and is used to provide pressurized air at 621 kPa. The ECU unit is connected to the air compressor and the pneumatic solenoid valves as shown in Fig. 4. For the evaporator and condenser of the cooling loop, two identical printed heat exchangers (Model: B3-014-12D-3.0, 12 plates) with a heat duty of 2 kW (water to water) and compatible with several refrigerants including the R134a (the refrigerant used in this study) are used. For the refrigerant expansion process, a needle-based expansion valve (EV) is used (Model: WINFLOW ¼” NPT [F], stainless steel).

To test the performance of the ECU-based refrigeration system in a controllable manner, the refrigerant evaporation and condensation processes are performed using circulating subsystems for hot and cold water, respectively (See Fig. 3). Each circulating water subsystem (CWS) consists of a pump (with a capacity of 100 – 275 L/h), control valve (CV), and insulated laboratory beaker. Also, each CWS is equipped with a water flow meter (100-1000L/H plastic tube type Water rotameter, model: LZS-15) and two K-type thermocouples (K-Type Thermocouple Probe Sensor 30 cm) to measure the inlet and outlet temperatures of the water. For the circuit of the cooling loop, four sets of thermocouple sensors and pressure gauges are used to measure the pressures and temperatures at the inlet and outlet of the evaporator and the condenser. An additional pressure gauge is installed in the end compressor chamber to measure the developed pressure by the ECU (P_{ECU}). Finally, a calibrated refrigerant flow meter (RFM, LZJ-10F Glass Tube Flowmeter) is installed at the exit of the condenser to measure the flow rate of the refrigerant. Fig. 4 shows the setup of the ECU-based refrigeration system and the measuring instruments and their precision are presented in Table 1.The details of the thermodynamic analysis of the present setup, testing procedures, and uncertainty analysis are presented in the next section.

Table 1
Measuring *instruments and their precision.*

Physical variable	Measuring device	Operating range	Accuracy
Pressure	Pressure gauges	0 kPa to 2482 kPa	± 1.6%
Temperature	Type K thermocouples	−50 °C to 1200 °C	± 0.2 °C
Refrigerant flow meter	LZJ-10F Glass Tube Flowmeter	3 L/min – 30 L/min	2.5%
Water flow meter	Water rotameter	100 L/h to1000 L/h	± 4%

4. Methodology

The methodology of the thermodynamic analysis of the experimental setup, testing procedures, validation, and uncertainty analysis are presented in this section.

4.1. Thermodynamic analysis

Four major parameters could be used to evaluate the performance of the ECU-based refrigeration system which are: (1) the developed pressure by the ECU (P_{ECU}), (2) the work rate of the ECU ($\dot{W}_{ECU}$), (3) the evaporation capacity (Q_{ev}), and (4) the coefficient of performance (COP) of the system. All of these parameters depend on the pressures and temperatures at the inlet and outlet of the condenser and the evaporator as well as the flow rate of the refrigerant (R134a). The first indicator P_{ECU} is obtained by the direct measurement using the pressure gauge at the bottom of the compressor chamber in the ECU (see Fig. 3). The second parameter ($\dot{W}_{ECU}$) is given as [29]:

$$\dot{W}_{ECU} = \dot{W}_{ECU,compr.} + \dot{W}_{ECU,\ suction} \tag{1}$$

where $\dot{W}_{ECU,compr.}$ and $\dot{W}_{ECU,\ suction}$ are the work rate to compress the refrigerant on the power stroke and the work rate to draw the refrigerant (and push the air in the expander cylinder) during the back-stroke, respectively. These work rates are defined as [18]:

$$\dot{W}_{ECU,compr.} = N \times L \times A \times (P_{ECU} - P_{ev,out}) \tag{2}$$

$$\dot{W}_{ECU,suction} = N \times L \times A \times P_{ev,out} \tag{3}$$

where N, L, A, and $P_{ev,out}$ are the operating frequency, stroke length, cross-sectional area of ECU, and the outlet evaporator pressure, respectively. Fig. 5 ((a) to (f)) shows the T-s, P-h, h-s, T-v, P-v, and T-h diagrams of the ECU-based refrigeration cycle at the initial test

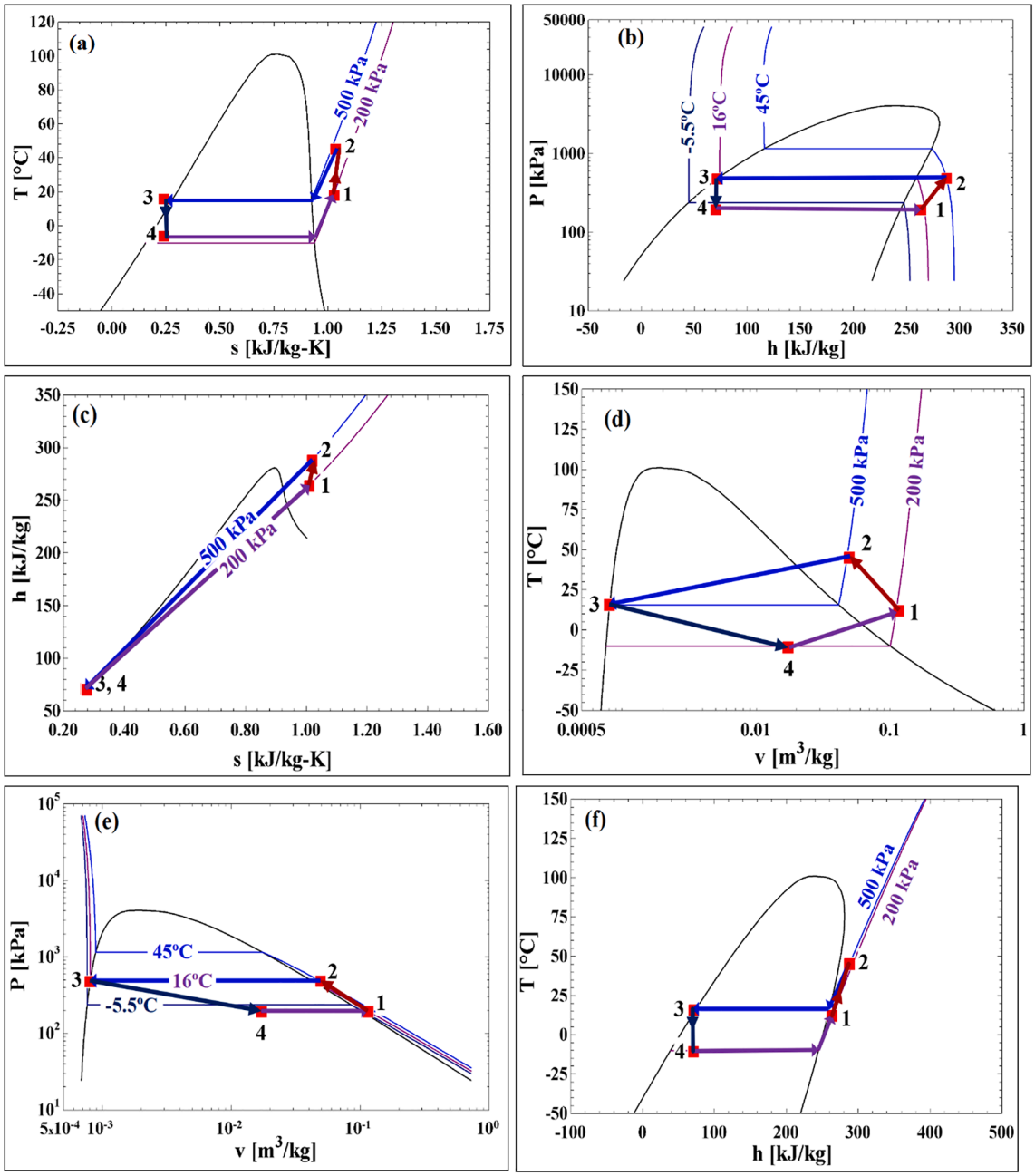

Fig. 5. (a) T-s, (b) P-h, (c) h-s, (d) T-v, (e) P-v, and (f) T-h diagrams of the ECU-based refrigeration cycle for the initial test.

conditions of the setup. In these subfigures, points 1, 2, 3, and 4 are the outlet of the evaporator, the inlet of the condenser, an outlet of the condenser, and the inlet of the evaporator, respectively. Based on Fig. 5 (a), the work rate of the ECU can be expressed in terms of the refrigerant flow rate and the refrigerant enthalpy difference through the compression process (1–2) as follows (see Fig. 6):

$$\dot{W}_{ECU} = \dot{m}_R \times (h_{2s} - h_1)/\eta_{comp.} \quad (4)$$

where $\dot{m}_R$ is the refrigerant flow rate, h_{2s} is the isentropic enthalpy of the refrigerant at the outlet of the ECU compressor chamber (the inlet of the condenser), h_1 is the enthalpy of the refrigerant at the inlet of the ECU compressor chamber (evaporator outlet), and $\eta_{comp.}$ is the isentropic efficiency of the ECU compressor chamber, which is defined as [30]:

$$\eta_{comp.} = (h_{2s} - h_1)/(h_{2a} - h_1) \quad (5)$$

where h_{2a} is the refrigerant enthalpy at the actual temperature at the inlet of the condenser.

The third performance indicator (Q_{ev}) is defined as:

$$Q_{ev} = \dot{m}_R \times (h_1 - h_4) \quad (6)$$

And the fourth indicator (COP) is defined as:

$$COP = Q_{ev}/\dot{W}_{ECU} \quad (7)$$

To ensure the accuracy of the setup measurements, the evaporation capacity is calculated based on the flow rate and temperature difference of the hot water passing through the evaporator as follows:

$$Q_{hot} = \dot{m}_{h,in} \times c_{p,avg} \times (T_{h,in} - T_{h,out}) \quad (8)$$

A significant part of the heat of the hot water (Q_{hot}) is absorbed by the refrigerant (Q_{ev}) and a small part is lost to the ambient air ($Q_{h,amb}$), thus:

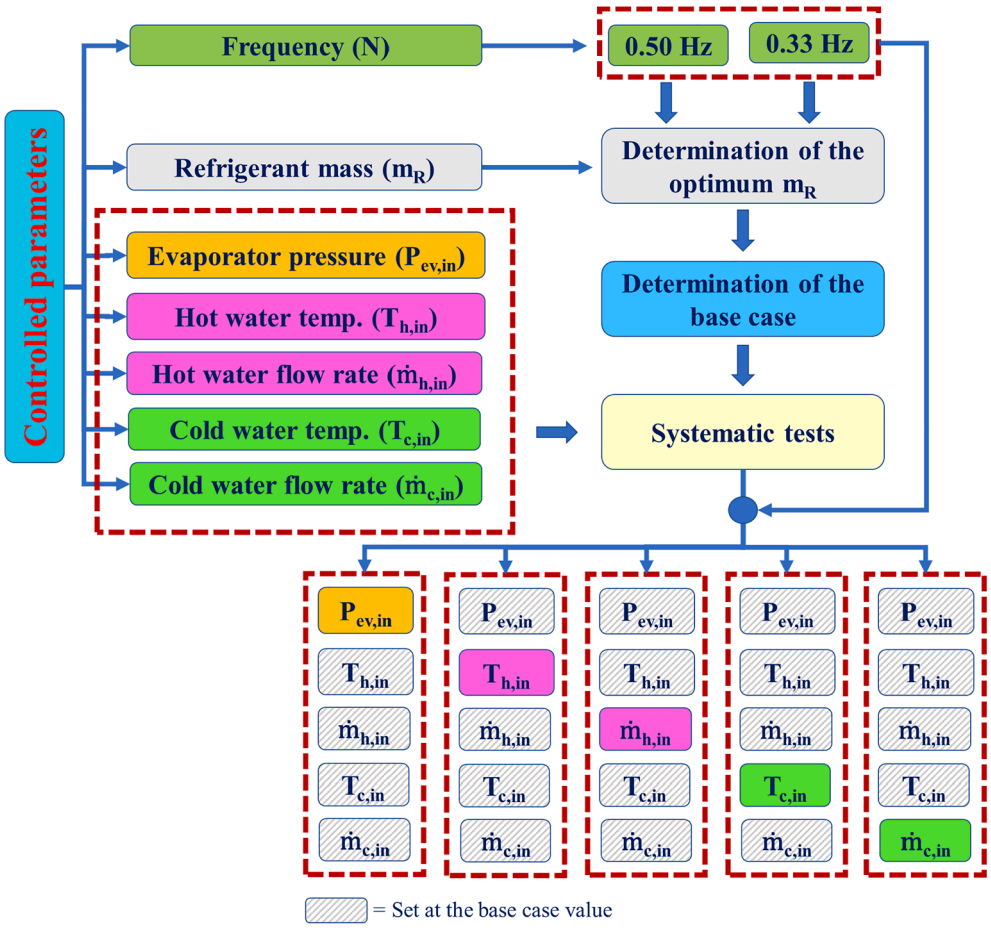

Fig. 6. Flow chart of the testing procedures.

$$Q_{hot} = Q_{ev} + Q_{h,amb} \quad (9)$$

The heat loss to the ambient air from the hot water to the ambient air through the surface area of the evaporator (as depicted in Appendix A (Fig. A.2)) is calculated as:

$$Q_{h,amb} = U_{h,amb} \times A_{h,amb} \times (T_{ev,avg} - T_{amb}) \quad (10)$$

where $U_{h,amb}$ is the heat transfer coefficient between the hot water and the ambient air, $A_{h,amb}$ is the surface area of the evaporator, $T_{ev,avg}$ is the average temperature of the hot water through the evaporator, and T_{amb} is the ambient temperature. A similar approach is applied to calculate the heat rejected by the refrigerant through the condensation process (Q_{co}) compared to that absorbed by the cold water (Q_{cold}) such that:

$$Q_{co} = \dot{m}_R \times (h_2 - h_3) \quad (11)$$

$$Q_{cold} = Q_{co} + Q_{c,amb} \quad (12)$$

$$Q_{c,amb} = U_{c,amb} \times A_{c,amb} \times (T_{amb} - T_{co,avg}) \quad (13)$$

where $U_{c,amb}$ is the heat transfer coefficient between the cold water and the ambient air, $A_{c,amb}$ is the surface area of the condenser, and $T_{co,avg}$ is the average temperature of the refrigerant through the condenser. The surface areas of the heat exchangers used as evaporator and condenser are identical and equal to ($A_{h,amb}$=$A_{c,amb}$ = 0.0557 m^2). Also, the heat transfer coefficients ($U_{h,amb}$, and$U_{c,amb}$) are calculated based on the equations presented in Appendix A at the average range of the operating conditions of the evaporator and condenser. For the base case (explained in section 5.1), $U_{h,amb}$=0.31 kW/m^2-^{o}C and$U_{c,amb}$ = 0.12 kW/m^2-^{o}C.

4.2. Testing procedures and validation

Seven operating parameters are used to control the operation of the ECU-based refrigeration system systematically, which are: (1) the operating frequency of the ECU (N), (2) the amount of the charged refrigerant mass to the cycle (m_R), (3) the inlet pressure of the evaporator ($P_{ev,in}$) by tuning the expansion valve, (4) the inlet temperature of the hot water ($T_{h,in}$), (5) the flow rate of the hot water ($\dot{m}_{h,in}$), (6) the inlet temperature of the cold water ($T_{c,in}$), and (7) the mass flow rate

Table 2
Validation of the thermodynamic calculations of the ECU-based refrigeration system*.

Parameter	Q_{ev}	$Q_{h,amb}$	Q_{hot}	Q_{co}	$Q_{c,amb}$	Q_{cold}	$\dot{W}_{ECU}$ [a]	$\dot{W}_{ECU}$ [b]
Unit	kW	kW	kW	kW	kW	kW	kW	kW
Value	0.42	0.13	0.55	0.47	0.07	0.54	0.1614	0.1632

* Calculated at ($P_{ev,in}$ = 193 kPa, $T_{h,in}$ = 33 °C, $\dot{m}_h$ = 170 L/h, $T_{c,in}$ = 11 °C, $\dot{m}_c$ = 275 L/h, and T_{amb} = 23 °C).
[a] Based-on Eqns. (1) to (3).
[b] Based-on Eqns. (4) and (5).

Table 3
Uncertainty results of the performance indicators.

Performance indicator	Uncertainty
P_{ECU}	± 1.60 % (±39.712 kPa)
$\dot{W}_{ECU}$	± 2.0% (±0.004 kw)
Q_{ev}	±3.4% (±0.02 kW)
COP	±4.0% (±0.1)

cold water ($\dot{m}_{c,in}$). First, for the first controlled parameter (N), the pneumatic solenoid valves are connected to a programmed control unit to operate the ECU at 0.50 Hz or 0.33 Hz. Then, for the charged refrigerant mass (m_R), a base case for the controlled parameters of the hot and cold water as well as the optimum amount of the refrigerant at each frequency is selected as discussed in section 5.1. The hot water temperature is controlled using a heater and the cold-water temperature is tunned using ice. The flow rates of both the hot and cold water are controlled using control valves as shown in Fig. 3. After that, the testing procedures of the other controlled apartments ($P_{ev,in}$, $T_{h,in}$, $\dot{m}_{h,in}$, $T_{c,in}$, and $\dot{m}_{c,in}$) were strategically designed to examine their effects of the performance indicators of the ECU-based refrigeration system as discussed in detail in section 5.2 to section 5.6.

To ensure the accuracy of the measurement, the calculated values for the evaporator capacity (Q_{ev}), and the condenser load (Q_{co}) calculated by the refrigerant data are compared to that of the lost by the hot water or gained by the cold water as shown in Table 2. Furthermore, the work rate of the ECU calculated based on the ECU frequency and developed pressure (Eqs. (1) to (3)) is compared to that calculated based on the refrigerant data (Eqs. (4) and (5)) as presented in Table 2. The results show that about 23% of the heat lost by the hot water is rejected to the ambient while 77% is absorbed by the evaporator. On the condenser, the heat gained by the cold water from the ambient air is 13% of the total gained heat through the condensation process. For the work rate of the ECU, there is a negligible difference between the calculated work rate from Eqs. (1) to (3) (0.1614 kW) to that from Eqs. (3) and (4) (0.1632 kW). It is worth to consider that if the volumetric efficiency is introduced to the work of the ECU in equations (1 to 3), then less work will be obtained as input for the cooling loop which yields higher values for its COP. However, to maintain conservative analysis approach, the work of the ECU was calculated at the full length of the stroke (100 mm).

4.3. Experimental uncertainty analysis

To verify the reliability of the experimental results, the relative uncertainty of the performance indicators (P_{ECU}, $\dot{W}_{ECU}$, Q_{ev}, and COP) are calculated using Eqns. (14) and (15) [2].

$$R = f(x_1, x_2, x_3, \cdots, x_n) \tag{14}$$

$$\sigma R = \frac{1}{R}\sqrt{\left(\frac{\partial R}{\partial x_1}\Delta x_1\right)^2 + \left(\frac{\partial R}{\partial x_2}\Delta x_2\right)^2 + \left(\frac{\partial R}{\partial x_3}\Delta x_3\right)^2 + \cdots + \left(\frac{\partial R}{\partial x_n}\Delta x_n\right)^2} \tag{15}$$

Therefore,

$\sigma P_{ECU} = \sqrt{\left(\frac{\delta P_{ECU}}{P_{ECU}}\right)^2} = \pm\frac{\delta P_{ECU}}{P_{ECU}}$ (13).

$$\sigma \dot{W}_{ECU} = \sqrt{\left(\frac{\delta N}{N}\right)^2 + \left(\frac{\delta L}{L}\right)^2 + \left(\frac{\delta A}{A}\right)^2 + \left(\frac{\delta P_{ECU}}{P_{ECU}}\right)^2 + \left(\frac{\delta P_{ev,out}}{P_{ev,out}}\right)^2} \tag{16}$$

$$\sigma Q_{ev} = \sqrt{\left(\frac{\delta \dot{m}_R}{\dot{m}_R}\right)^2 + \left(\frac{\delta T_{ev,in}}{T_{ev,in}}\right)^2 + \left(\frac{\delta T_{ev,out}}{T_{ev,in}}\right)^2 + \left(\frac{\delta P_{ev,in}}{P_{ev,in}}\right)^2 + \left(\frac{\delta P_{ev,out}}{P_{ev,in}}\right)^2} \tag{17}$$

$$\sigma COP = \sqrt{(\sigma Q_{ev})^2 + (\sigma \dot{W}_{ECU})^2} \tag{18}$$

The results of the uncertainty analysis for the performance indicators are presented Table 3.

5. Results and discussion

In this section, the details of the testing process and the performance indicators are presented and discussed based on the measurement data.

5.1. Effect of the refrigerant mass

To establish the base case of the controlled parameters ($P_{ev,in}$, $T_{h,in}$, $\dot{m}_h$, $T_{c,in}$, and $\dot{m}_c$), the ECU setup is charged by 60 g of R134a and operated at 0.50 Hz. Then, the controlled variables are regularly changed and recorded with time as shown in Fig. 7 (a, and b). This means that the recorded data in Fig. 7 were generated to initialize the base case values of the controlled variables and not to realize steady state mode of the system. Based on the generated data in Fig. 7 (a, and b), the COP and the evaporator capacity of the ECU-based refrigeration system are calculated as shown in Fig. 7 (c). For the data from 9:36 to 11:15, the evaporator pressure is increased with a marginal variation on the other parameters. After that (from 11:15 to 12:25), the hot water temperature is increased (from 15 °C to 50 °C) with the full capacity of the pump (275 L/h). Then, the temperature of the hot water readjusted at 33 °C and after some time, the cold-water temperature is decreased from 20 to −0.30 °C (from 13:55 to 14:45). Finally, both the cold and hot inlet temperatures were adjusted at 12 °C and 30 °C at the full capacity of the pumps (from 14:55 to 15:55). It is found that higher COP (up to 2.60) is noted at a hot water flow rate of 150 L/h with an average inlet temperature of 33 °C and cold-water flow rate of 250 L/h and average inlet temperature of 15 °C. Therefore, the base case of the controlled variables is determined as ($P_{ev,in}$ = 20 psi = 137 kPa, $T_{h,in}$ = 33 °C, $\dot{m}_h$ = 150 L/h, $T_{c,in}$ = 15 °C, and $\dot{m}_c$ = 275 L/h). It is worth mentioning that to maintain the setup compactness, the hot water on the evaporator side is used with much higher temperatures than water on the condenser side. In this way, high cooling load is provided to the evaporator by increasing the temperature difference between the hot water and the refrigerant streams rather than increasing the size of the evaporator.

As the refrigerant mass plays a key role in the vapor compression of the refrigerant, it is an essential step to determine the optimum amount of the refrigerant to be charged at 0.50 Hz and 0.33 Hz operation. Therefore, the ECU setup is first evacuated using an evacuation pump, then the refrigerant is charged starting from 40 g and gradually increased up to 100 g. At each charged mass, the setup is running at 0.50 Hz and 0.33 Hz. Then, the performance indicators are calculated and presented with the charged mass as shown in Fig. 8 for 0.50 Hz and Fig. 9 for 0.33 Hz. For 0.50 Hz, it is found that the increase of the refrigerant mass first increases the work rate of the ECU up to 50 g then decreases it for further increase. However, the evaporator capacity is increased up to 60 g then declines for higher charged mass. Therefore, the optimum COP at 0.50 Hz is achieved at a refrigerant mass of 60 g. At charged mass higher than 60 g, a significant increase of the evaporator temperature is noted, which increases the specific volume of the refrigerant and thus reduces the developed pressure by the ECU. At 0.33 Hz, the increase of the evaporator pressure is noted at refrigerant mass higher than 80 g. Therefore, for the investigation of the controlled variable effects on the performance indicators of the ECU-based refrigeration system, the operation at 0.50 Hz is performed with a charged mass of 60 g and with 80 g at 0.33 Hz.

5.2. Effect of the evaporator pressure

To examine the effect of the evaporator inlet pressure on the performance indicators of the ECU-based refrigeration system, the hot was maintained at an average inlet temperature of 33 °C and flow rate of 150 L/h. Also, the cold water was maintained at an average inlet temperature of 15 °C and a flow rate of 250 L/h. Then, the expansion valve was

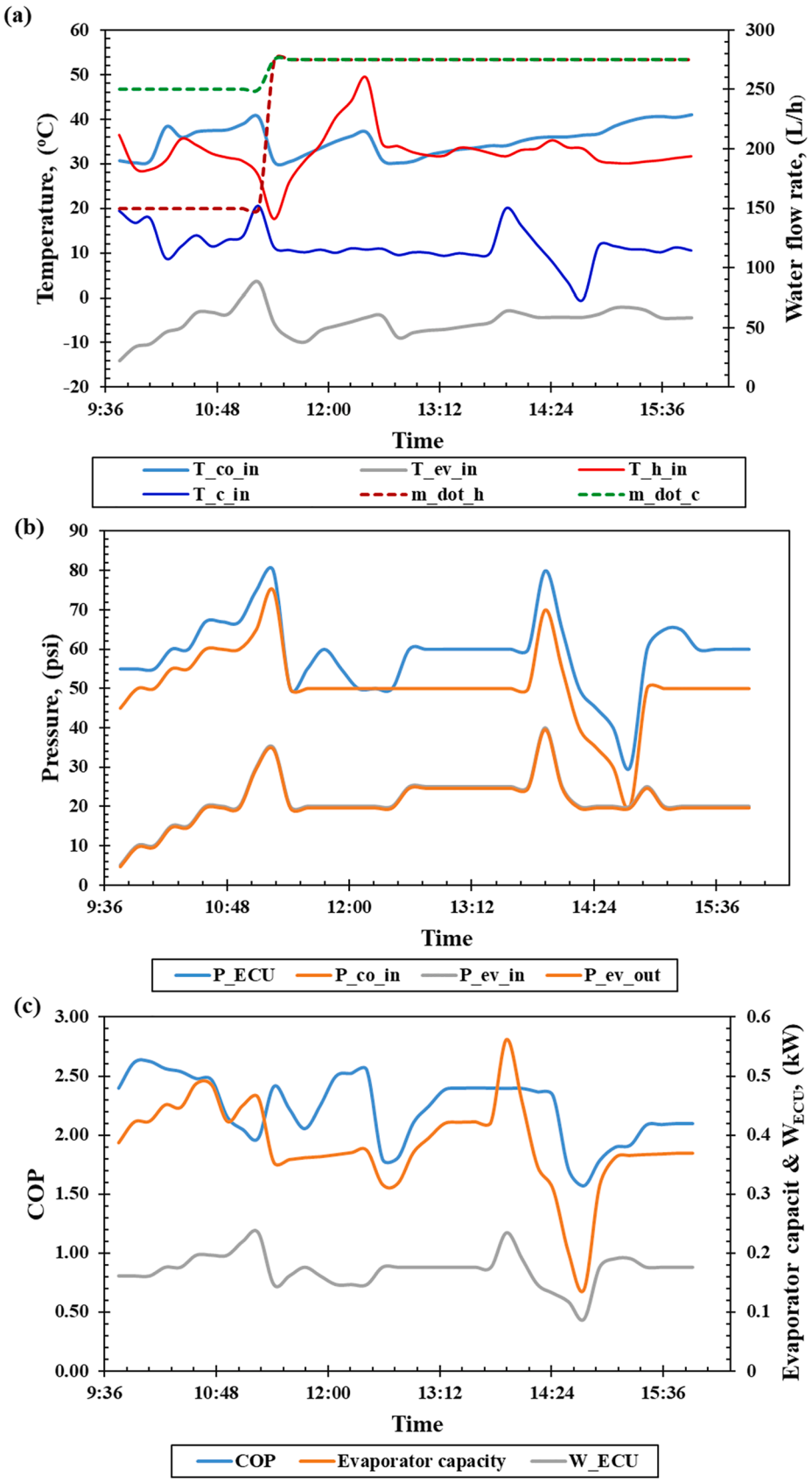

Fig. 7. Initial test of the ECU-based refrigeration system. Note: the purpose of the data generated in this figure is to initialize the base case values of the controlled variables and not to realize steady state mode of the system.

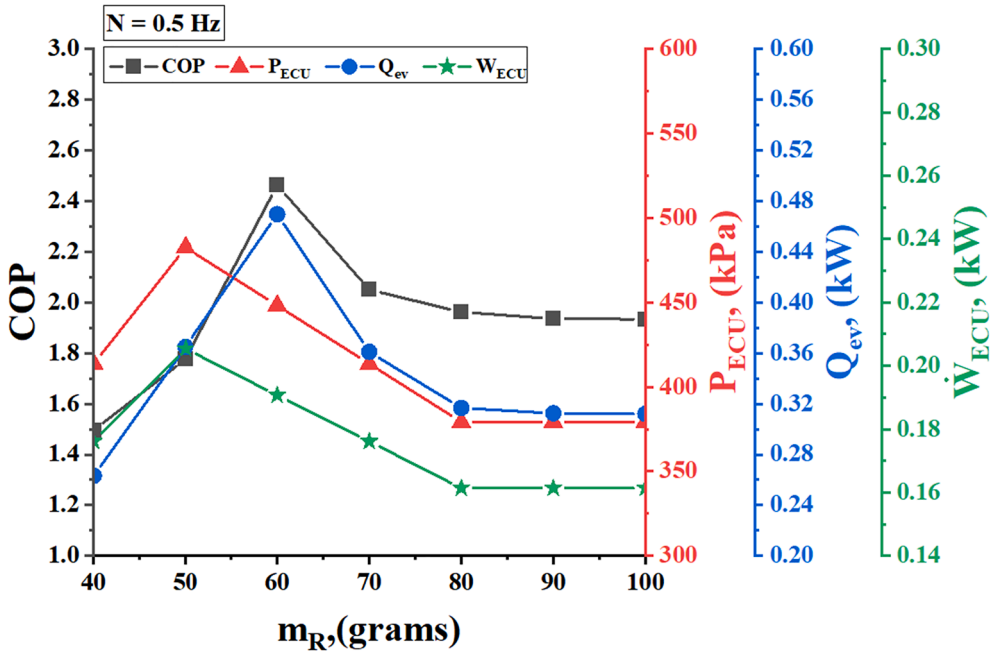

Fig. 8. Variation of the performance indicators with the refrigerant charged mass at 0.50 Hz.

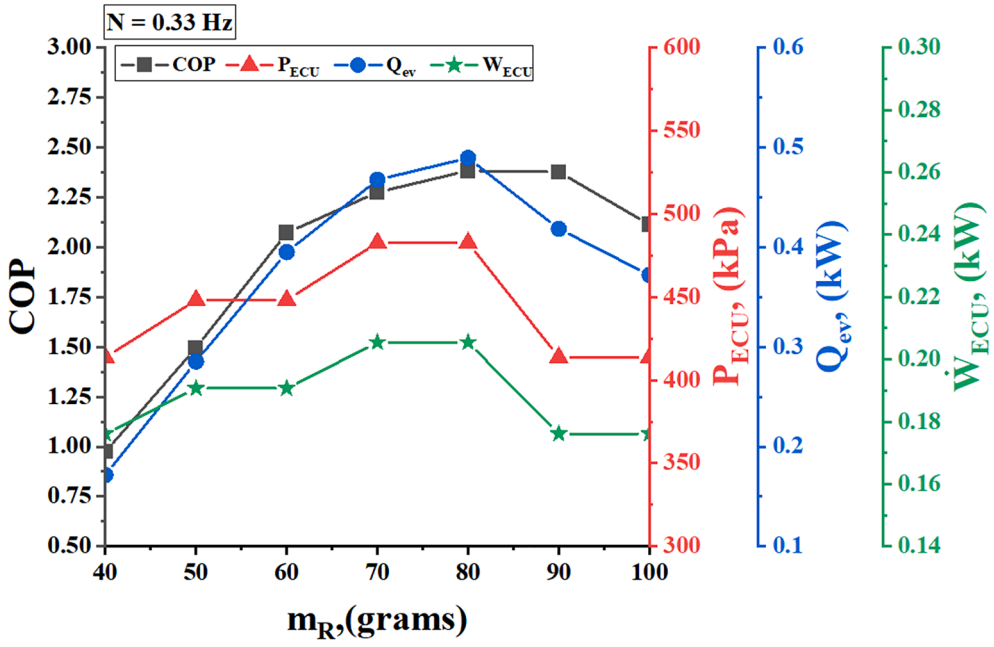

Fig. 9. Variation of the performance indicators with the refrigerant charged mass at 0.33 Hz.

adjusted for five evaporator inlet pressures which are 35, 69, 103, 138, 209, and 241 kPa. Then, the performance indicators are calculated based on the measured pressures, temperatures, and flow rate and presented in Fig. 10 (a) at a frequency of 0.50 Hz and charged refrigerant mass of 60 g. It is found that the developed pressure by the ECU unit and thus its work rate proportionally increases with the increases of the evaporator pressure, which, in turn, increases the refrigerant flow rate as shown in Fig. 10 (b). Simultanously, the enthapy difference through the evaporator ($h_1 - h_4$) decreases with the increase of the evaporator pressure with sharpre decrease at pressure higher than 137 kPa (see Fig. 10 (b)). This implies that the increase of the refrigerant flow rate is the dominant effect up to evaporator pressure of 137 kPa which increases the evaporator cooling capacity from 0.39 kW to 0.49 kW. These cooling capacities are obtained with evaporator temperatures of −14 °C to −3.4 °C. At higher evaporator pressure, the enthalpy difference reduction dominates the evaporator capacity and reduces it to 0.45 kW. Therefore, the ratio of the evaporator capacity to the ECU work rate (COP) first increases (up to 69 kPa), then decreases for further increase in the evaporator pressure. This implies that the evaporator pressure should be minimized for optimal operation of the ECU system. However, if a larger evaporator capacity is needed, then the evaporator pressure can be increased with the penalty of reduction on the COP of the cooling loop.

As the setup is running with a frequency of 0.33 Hz with no change on the charged refrigerant mass, it is noticed that there is no cooling effect achieved; as the inlet evaporator temperature was higher than

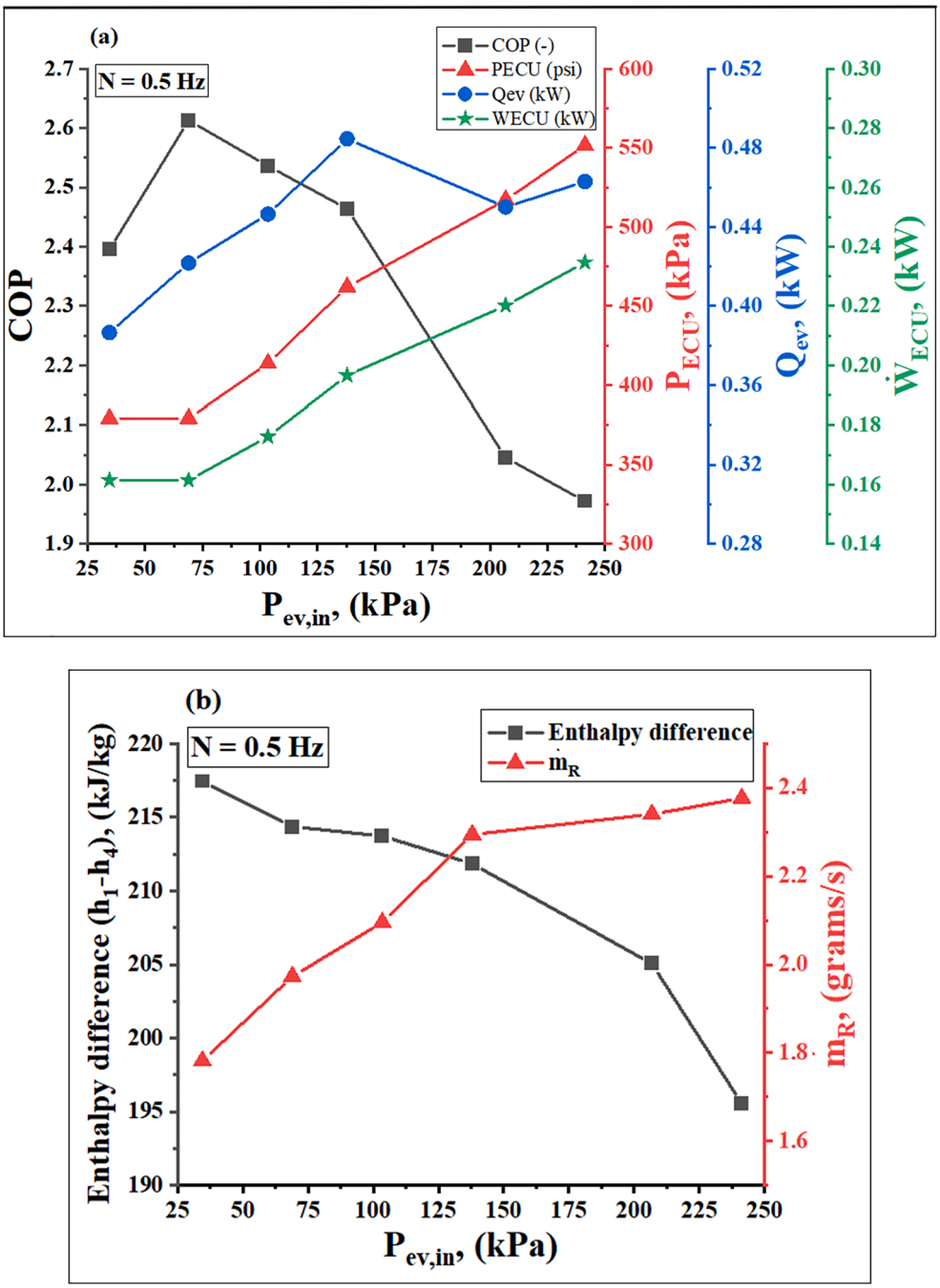

Fig. 10. Variation of (a) the performance indicators, and (b) refrigerant flow rate and evaporator enthalpy difference (h_1-h_4) with the evaporator inlet pressure at 0.50 Hz.

13 °C. It is assumed that the cooling effect is achieved if the evaporator temperature is below (0 °C). Therefore, the refrigerant mass is increased until a cooling effect is achieved by reaching an evaporator inlet temperature of −9.6 °C at a refrigerant mass of 80 g. Then, the evaporator inlet pressure is changed (by adjusting the expansion valve) and the performance indicators are calculated and presented in Fig. 11. It can be noted that the cooling effect at 0.33 Hz is achieved over a smaller range of evaporator pressure (103 – 241 kPa) than at 0.50 Hz (34 – 241 kPa). However, the COP at 0.33 Hz does not sharply decrease with the increase of the evaporator pressure as at 0.50 Hz. For instance, as the evaporator pressure increases from 103 kPa to 241 kPa, the COP decreases from 2.54 to 1.97 at 0.5 Hz, and from 2.47 to 2.37 at 0.33 Hz. This is because that the ECU builds pressure at 0.33 Hz comparable to that of 0.50 Hz which yields almost the same cooling capacities (0.43 to 0.48 kW) with less work rate. The work rate at 0.50 Hz increases from 0.18 kW to 0.23 kW compared to 0.18 kW to 0.21 kW at 0.33 Hz over an evaporator pressure of 103 kPa to 241 kPa. Therefore, as concluded from Table 4, it can be stated that the operation of the ECU at a higher frequency (0.5 Hz) is preferred for low evaporator pressure (less than 100 kPa) and temperature less than −10 °C while lower frequency operation is more efficient for higher evaporator pressure (higher than 100 kPa) and evaporator temperatures higher than −10 °C).

5.3. *Effect of hot water temperature*

The effect of the hot water inlet temperature is tested at an

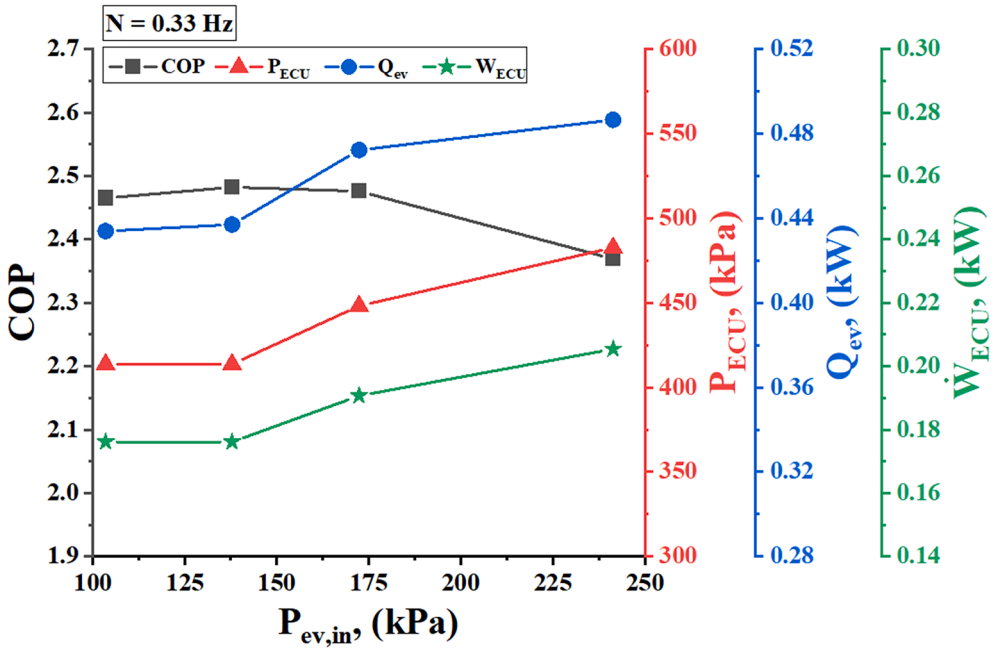

Fig. 11. Variation of the performance indicators with the evaporator inlet pressure at 0.33 Hz.

Table 4
Comparison of the ECU operation at frequencies of 0.33 Hz and 0.50 Hz for the variation of the evaporator inlet pressure.

Parameter	For 0.33 Hz	For 0.50 Hz
$P_{ev,in}$, (kPa)	103 – 241	34 – 241
$T_{ev,in}$, (°C)	−9.6– −3.4	−14 – −3.4
P_{ECU}, (kPa)	414 – 483	379 – 552
Q_{ev}, (kW)	0.43 – 0.48	0.38 – 0.48
$\dot{W}_{ECU}$, (kW)	0.18 – 0.21	0.16 – 0.23
COP	2.37 – 2.48	1.97 – 2.61

evaporator pressure of 137 kPa. The hot water flow rate is set as 150 L/h and the cold water was maintained at an average inlet temperature of 15 °C and flow rate of 250 L/h. Then, the how water temperature is gradually increased from 26 °C to 49 °C. As shown in Fig. 12, the developed pressure by the ECU (P_{ECU}) first decreases from 483 kPa to 344 kPa as the hot water temperature increased from 26 °C to 40 °C. Then, the P_{ECU} remains at 344 kPa at higher hot water temperatures up to 49 °C. The decreare of P_{ECU} with the increase of hot water temperature (from 13.2 °C to 31.5 °C) is caused by the corresponding increase of the refrigerant straem at the exit of the evaporator. This means that higher hot water temperature yields higher refrigerant temperature and lower density (reduced from 6.25 kg/ m^3 to 5.56 kg/ m^3) of the refrigerant at the inlet of the ECU. This, in turn, reduces the P_{ECU} as the

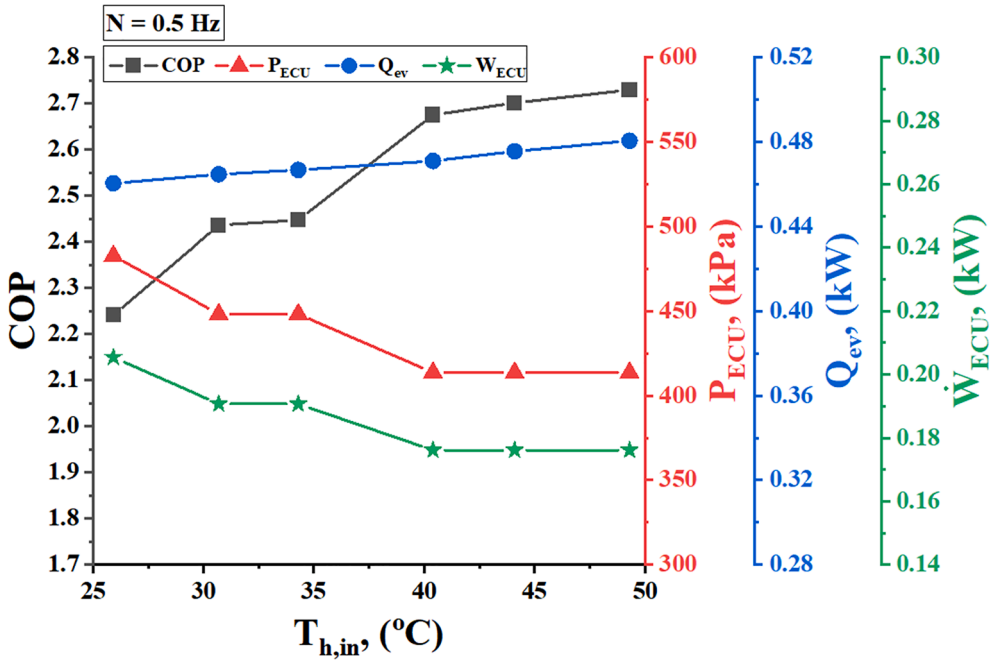

Fig. 12. Variation of the performance indicators with the hot water inlet temperature at 0.5 Hz.

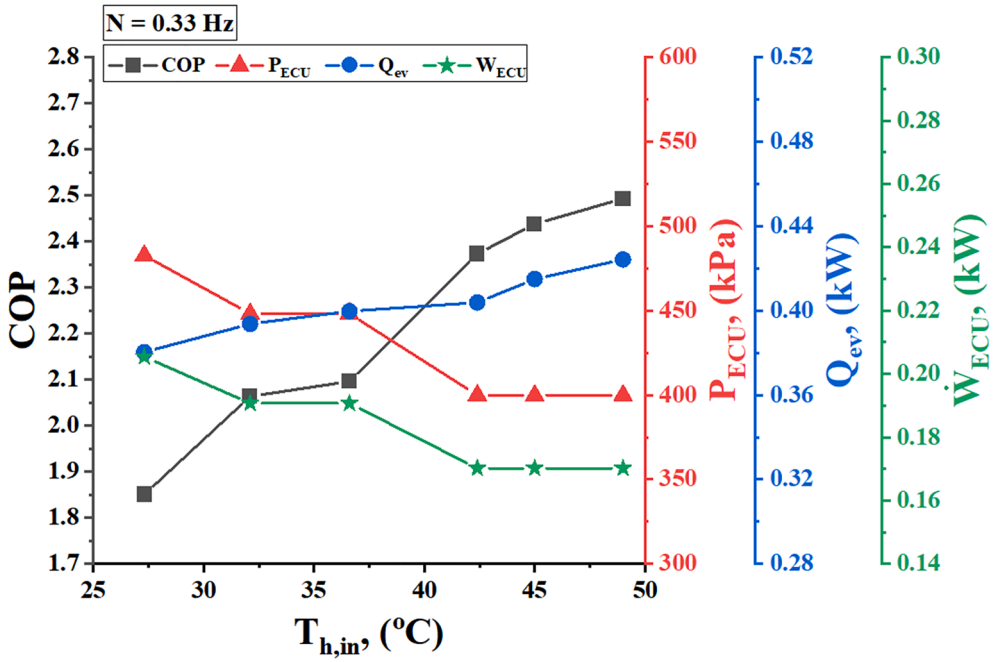

Fig. 13. Variation of the performance indicators with the hot water inlet temperature at 0.33 Hz.

Table 5
Comparison of the average values of the performance indicators ats the frequency reduces from 0.50 Hz and 0.33 Hz for the variation of the hot inlet temperature variation from 26 °C to 49 °C.

Parameter	For 0.50 Hz	For 0.33 Hz	Reduction percent (%)
P_{ECU}, (kPa)	436	429	1.61
Q_{ev}, (kW)	0.47	0.40	14.89
$\dot{W}_{ECU}$, (kW)	0.19	0.18	5.26
COP	2.54	2.22	12.59

refrigerant as the build up pressure by the ECU strongly affected by the density of the compressed refrigernat. On the other side, as the hot water temperature increases, the temperature difference between the hot water and refrigerant through the heater also increased from 12.7 °C to 17.8 °C, which enhances the heat transfer process to the refrigerant and increases the evaporator capacity from 0.46 kW to 0.48 kW. Therefore, the COP is improved at higher cooling loads as it increases from 2.2 to 2.7 over the range of the hot water inlet temperature. However, the COP is slightly improved at hot water temperatures higher than 40 °C.

As the frequency is decreased to 0.33 Hz, the behavior of the performance indicators is similar to that at 0.50 Hz as shown in Fig. 13. But the refrigerant flow rate reduces from an average of 9 L/min at 0.50 Hz to 7.45 L/min Hz at 0.33 Hz. This reduces the cooling capacity of the

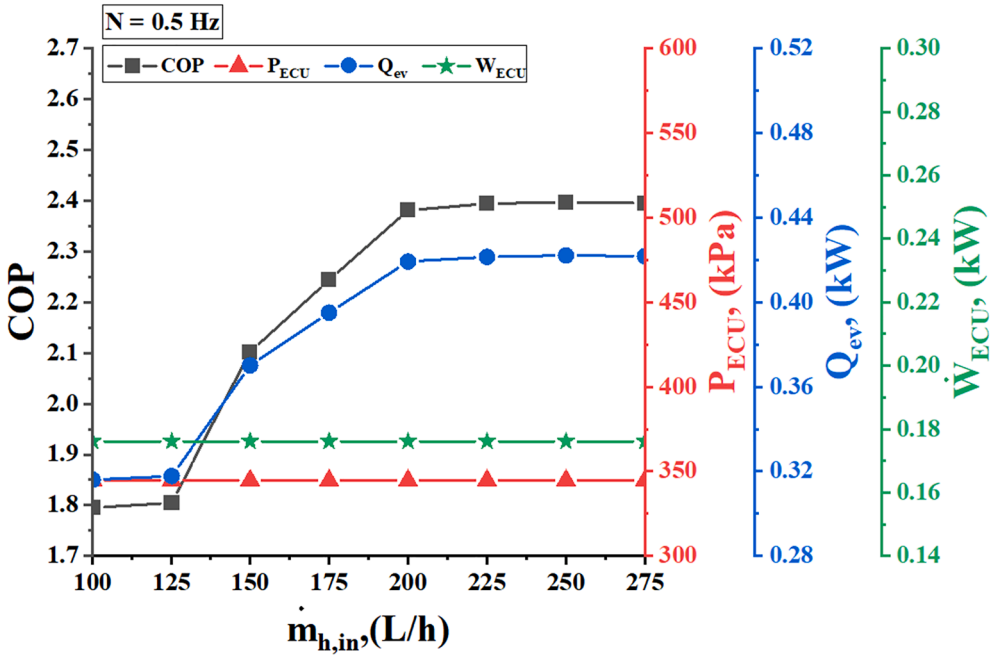

Fig. 14. Variation of the performance indicators with the hot water flow rate at 0.5 Hz.

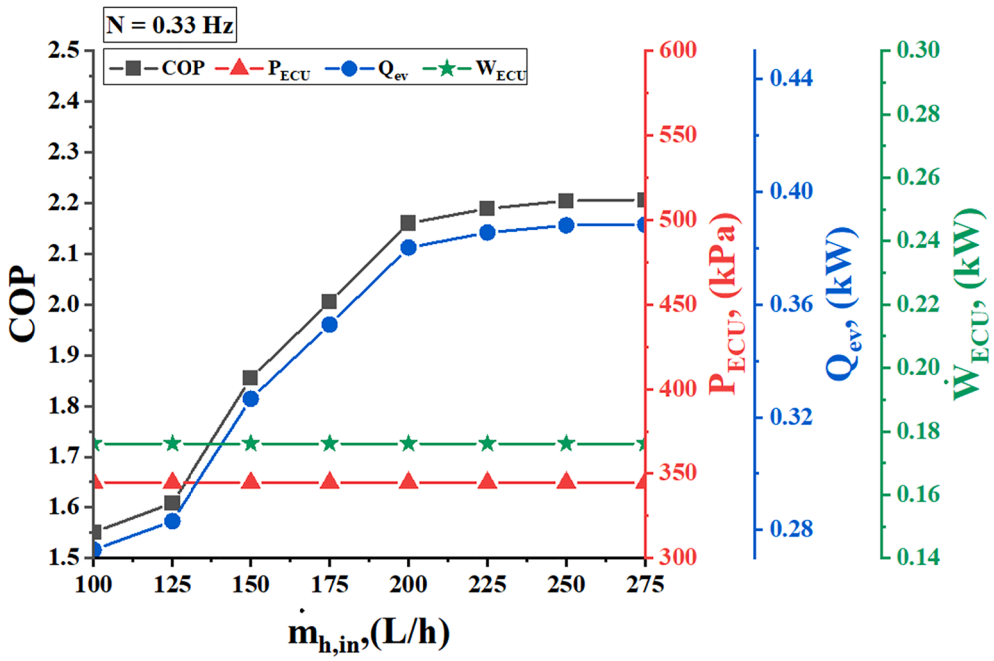

Fig. 15. Variation of the performance indicators with the hot water flow rate at 0.33 Hz.

evaporator from an average of 0.47 kW at 0.50 Hz to 0.40 kW at 0.33 Hz. At the same time, the work rate of the ECU reduces from 0.19 kW at 0.50 Hz to 0.18 kW at 0.33 Hz. However, the reduction of the cooling capacity is more dominant than the reduction of the work rate of the ECU. Thus, the COP is reduced from an average of 2.54 at 0.50 Hz to 2.22 at 0.33 Hz. Table 5 summarises the average values of the performance indicators at 0.50 Hz and 0.33 Hz and shows the percent of reduction on each indicator that yields due to the frequency decrease.

5.4. Effect hot water flow rate

To investigate the effect of the hot water flow rate ($\dot{m}_h$), it is gradually increased (using the control valves shown in Fig. 3) from 100 L/h to 275 L/h, while the other controlled variables were maintained at $P_{ev,in}$ = 137 kPa, $T_{h,in}$ = 33 °C, $\dot{m}_c$ = 250 L/h, and $T_{c,in}$ = 15 °C. At these conditions, the performance indicators at 0.50 Hz and 0.33 Hz are changed as shown in Fig. 14 and Fig. 15, respectively. It is found that the increase of $\dot{m}_h$ slightly reduces the work rate of the ECU at both 0.50 Hz and 0.33 Hz cases. This occurs due to the reduction of the pressure developed by the ECU as the specific volume of the refrigerant slightly increases with the increase of $\dot{m}_h$. Simultaneously, the evaporator temperature increases from −8.8 °C to −5.4 °C over the tested range of $\dot{m}_h$. As the refrigerant R134a behaves as an isentropic refrigerant, its evaporation capacity increases with the increase of the evaporator temperature. Therefore, the evaporation capacity is increased from 0.32 kW to 0.42 kW at 0.50 Hz and from 0.27 kW to 0.38 kW at 0.33 Hz. Furthermore, the evaporation capacity for both frequencies slightly changes at $\dot{m}_h$ higher than 200 L/h. Thus, it can be said that the evaporator reaches its full capability at $\dot{m}_h$ of 200 L/h, $P_{ev,in}$ = 137 kPa, and $T_{h,in}$ = 33 °C. However, higher evaporation capacity could be reached at $T_{h,in}$ higher than 33 °C and $\dot{m}_h$ lower than 200 L/min. For instance, as shown in Fig. 12, the evaporation capacity was 0.48 kW at $\dot{m}_h$ of 150 L/h, $P_{ev,in}$ = 137 kPa, and $T_{h,in}$ = 49 °C. This implies that the larger temperature difference between the hot water and the refrigerant improves the evaporation capacity more than the increase of the flow rate of the hot water. The average cooling capacity and work rate of the ECU are 0.39 kW and 0.18 kW, respectively, at 0.50 Hz while at 0.33 Hz are 0.17 kW and 0.35 kW. Therefore, the average COP at 0.50 Hz (2.2) is about 4.7% higher than at 0.33 Hz (2.1). This emphasizes that the operation of the ECU unit at a higher frequency yields higher evaporation capacity and improves the COP of the refrigeration cycle. Moreover, higher frequency maintains the refrigerant of the flow as a continuous flow through the cycle rather than the pulses flow observed at 0.33 Hz.

5.5. Effect of the cold-water temperature

Fig. 16 (a) and Fig. 17 show the effect of the cold-water temperature that is used for the condensation process on the performance indicators of the ECU-based refrigeration cycle at 0.50 Hz and 0.33 Hz, respectively. For this test, the other controlled variables were adjusted as $\dot{m}_h$ = 150 L/h, $\dot{m}_h$ = 250 L/h, $P_{ev,in}$ = 137 kPa, $T_{h,in}$ = 33 °C.

As the cold-water inlet temperature ($T_{c,in}$) reduces from 20 °C to around 0 °C, the evaporator temperature also decreases from −5.3 °C to −9.6 °C at 0.50 Hz and from −5.3 °C to −9.2 °C at 0.33 Hz. Lower evaporator temperatures followed by lower pressure and higher enthalpy difference through the evaporator, as shown in Fig. 16 (b). However, lower evaporator pressure reduces the build up pressure of the ECU as the supplied pressure of the compressed air was kept constant. With lower P_{ECU}, the flow rate of the refrigerant is decreases as shown in Fig. 16 (b). Therefore, the evaporation capacity and the work rate are reduced with the decrease of the $T_{c,in}$. At 0.50 Hz, the slope of evaporation capacity decline is close to that of the ECU work rate which yields a levelized COP (2.38) as the $T_{c,in}$ reduces from 20 °C to 8 °C with an optimum COP of 2.39 at $T_{c,in}$ of 16 °C. At $T_{c,in}$ less than 4 °C, a significant reduction in the evaporation capacity is noticed compared to a small reduction in the ECU work rate, thus, the COP reduces from 2.33 at $T_{c,in}$ of 8 °C to 1.71 at $T_{c,in}$ of 4 °C. On the other side, at 0.33 Hz, the reduction of the evaporation capacity was proportional to the reduction of the ECU work rate. This is because the reduction of the frequency affects both the work rate as well as the flow rate of the refrigerant. Therefore, the COP is reduced from 2.39 to 1.56 at 0.33 Hz. Therefore, it can be concluded that the ECU works efficiently at water temperatures higher than 15 °C for the refrigerant condensation process.

Table 6 compares the results of increasing the hot water temperature ($T_{h,in}$) to the decrease of the cold-water temperature ($T_{c,in}$). On one hand, it is found that the increase of $T_{h,in}$ (from 26 °C to 49 °C) reduces the work rate of the ECU ($\dot{W}_{ECU}$) and increases the evaporator capacity, thus improving the COP by 21% at 0.50 Hz and 35% at 0.33 Hz. On the

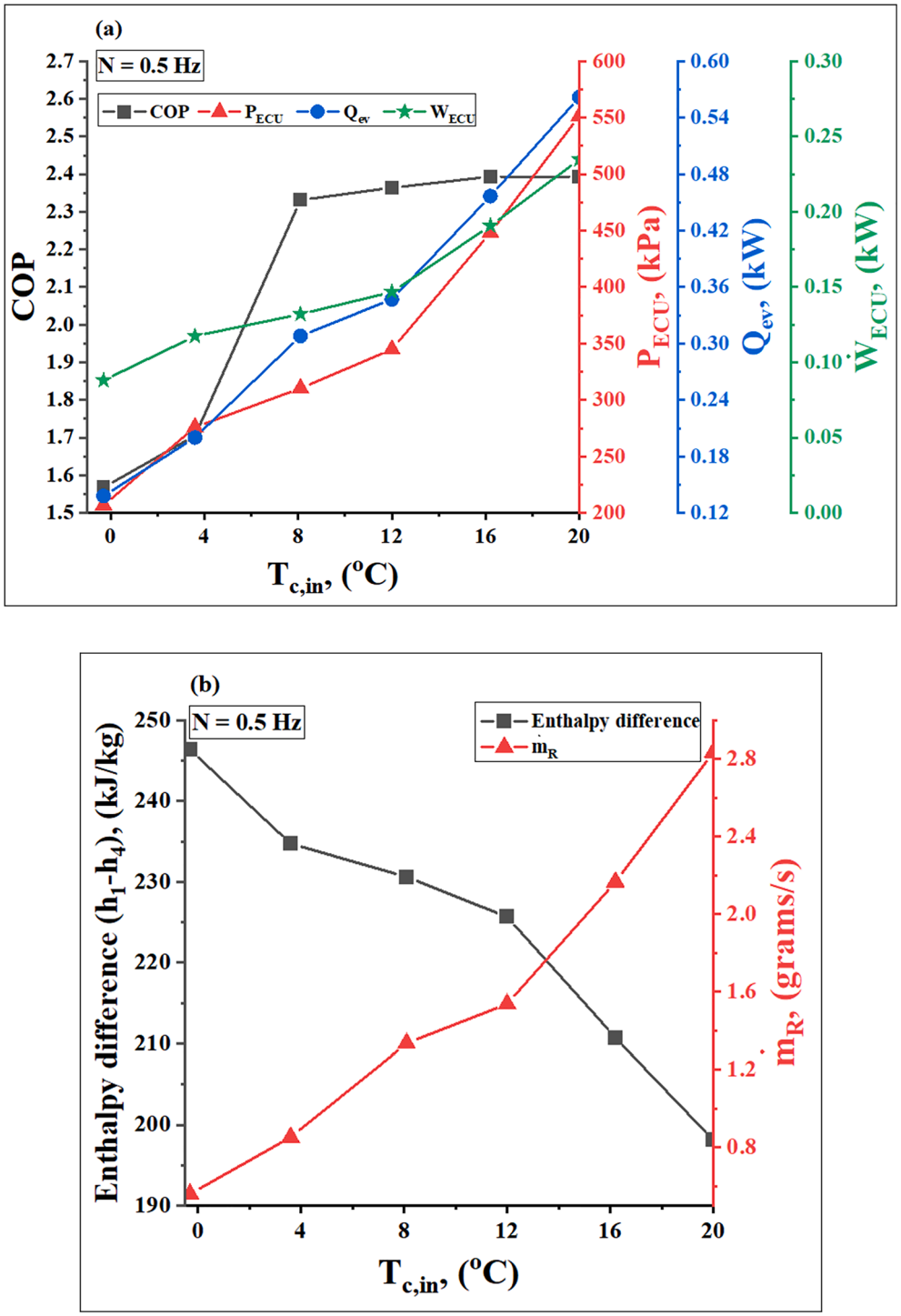

Fig. 16. Variation of (a) the performance indicators, and (b) refrigerant flow rate and evaporator enthalpy difference (h_1-h_4) with the cold-water inlet temperature at 0.5 Hz.

other hand, the decrease of $T_{c,in}$ (from 20 °C to 0.1 °C) reduces both the $\dot{W}_{ECU}$ and the evaporator capacity which reduces the COP by 34% at 0.50 Hz and by 32% at 0.33 Hz. Based on the average performance parameters over the ranges of $T_{h,in}$, and $T_{c,in}$, the average evaporator capacity with $T_{h,in}$ increase is 38% higher than for $T_{c,in}$ decrease as shown in Fig. 18. While, at 0.33 Hz, the average evaporator capacities are the same for both $T_{h,in}$ increase and $T_{c,in}$ decrease. However, due to the difference in the ECU work rate, the average COP due to $T_{h,in}$ increase is higher than due to $T_{c,in}$ decrease by 11% at 0.50 Hz and by 16% at 0.33 Hz.

5.6. *Effect of the cold-water flow rate*

In contrast to the increase of the hot water flow rate ($\dot{m}_h$), the increase of the cold-water flow rate ($\dot{m}_c$) (using the control valves shown in Fig. 3) slightly changes the evaporation capacity and significantly reduces the ECU work rate. This is due to the slight variation of the evaporator temperature (less than 2 °C) with an increase in the specific volume of the refrigerant at the inlet of the ECU (from 0.13 m^3/kg to 0.17 m^3/kg). Therefore, the evaporation capacity is levelized at 0.37 kW for cold-water flow rate higher than 125 L/h at 0.50 Hz and 0.35 kW

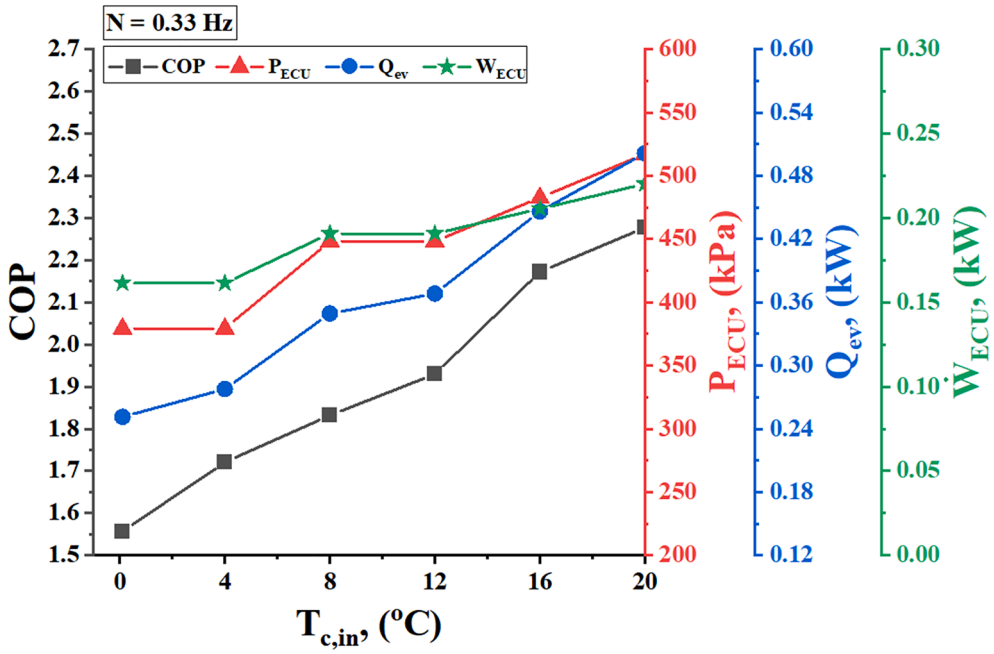

Fig. 17. Variation of the performance indicators with the cold-water inlet temperature at 0.33 Hz.

Table 6
Comparison between the effect of the increase of the hot water temperature and the decrease of the cold-water temperature on the performance indicators of the ECU.

Parameter	$T_{h,in}$ increase (26 °C to 49 °C)		$T_{c,in}$ decrease (20 °C to 0.5 °C)	
	0.50 Hz	0.33 Hz	0.50 Hz	0.33 Hz
P_{ECU}, (kPa)	482 – 413	483 – 400	551 – 206	517 – 379
Q_{ev}, (kW)	0.46 – 0.48	0.38 – 0.42	0.56 – 0.14	0.50 – 0.25
$\dot{W}_{ECU}$, (kW)	0.21– 0.18	0.21 – 0.17	0.23 – 0.09	0.22 – 0.16
COP	2.24 – 2.73	1.85 – 2.49	2.39 – 1.57	2.28 – 1.56

over the full range of the cold-water flow rate at 0.33 Hz (see Fig. 19 and Fig. 20). Also, the increase of the $\dot{m}_c$ significantly reduces the work rate of the ECU from 0.21 kW to 0.18 kW at 0.50 Hz and from 0.20 kW to 0.16 kW at 0.33 Hz as $\dot{m}_c$ increases from 100 L/h to 175 L/h. Then, the work rate is levelized at a constant value for $\dot{m}_c$ higher than 200 L/h for both frequencies. Thus, it can be concluded the significant reduction of the evaporator temperature (higher than 5 °C) obtained by the decrease of $T_{c,in}$ (discussed in section 5.5) reduces both the work rate of the ECU and the evaporator capacity. While the increase of $\dot{m}_c$ slightly changes the evaporator capacity with a significant reduction (17%) on the work rate of the ECU. Therefore, to enhance the COP of the ECU-based system through the condensation process, it should be performed by increasing the flow rate of the cooling fluid rather than reducing its temperature.

5.7. Comparison

Comparison between the features and limitations of the conventional TMR systems (Ejector-based and ORC-based) systems with those of the present ECU-based system is presented in Table 7. The ORC is a amateur technology, operates efficiently at temperatures lower than 300 °C and it could be designed in a very broad range of capacities. However, it is not economical at temperatures lower than 100 °C. Also, the design of expander still requires more improvements to enhance the cycle efficiency. The main advantages of the ejector-based systems are their structure simplicity and low cost. However, they suffer from low COP and complex design process. Therefore, the ECU-based TMR systems overcomes these limitations enjoying its simplicity, flexibility in the cooling capacity, and efficient operability even at an ultra-low heat source with a minimum temperature of 70 °C. From the aforementioned results, it is clear that the ECU-based refrigeration system provides a cooling load with evaporation temperature up to less than −10 °C with COP varies between from 1.50 to 2.60. This implies that the average COP of the present ECU-based system (2.05) is three times higher than the average COP of the ejector-based systems (0.62) and 2.70 times higher than that of the ORC-based systems (0.75) [6]. Furthermore, the COP of the ECU-based system is comparable for the double-mode electric-based refrigeration system, which varies from 1.42 to 5.20 at evaporation temperature of −35 °C to 10 °C at a condensation temperature of 35 °C [31,32].

6. Conclusions

This work presents a systematic experimental investigation on the performance of an innovative thermo-mechanical refrigeration (TMR) system. The theoretical TMR system integrates a power loop (powered by a low-grade heat source (up to 70 °C)) and a cooling loop using an expander-compressor unit (ECU). The ECU converts the thermal energy of the pressurized fluid of the power loop into mechanical energy to compress the refrigerant of the cooling loop. In the experimental setup of the present work, an air compressor is used to drive the ECU at a supply pressure of 620 kPa. Then, using R134a as a refrigerant, the ECU-based refrigeration system was systematically tested using hot circulated water for the evaporation process and cold circulated water for the condensation process. Several operating conditions are tested to investigate their influences on the performance indicators of the ECU-based system including the ECU developed pressure, ECU work rates, evaporation capacity, and the coefficient of performance (COP) of the cooling cycle. The main findings of the present work can be summarized as follows:

- For the operation of the ECU-based system with COP higher than 2, the optimal mass refrigerant must be determined, and the cooling loop should be adjusted to work at low evaporator pressure (less than150 kPa) with the high-frequency mode (0.5 Hz). At higher evaporator pressure, the low-frequency operation is recommended for larger evaporation capacity (>0.44 kW)with the penalty of lower COP (less than2).

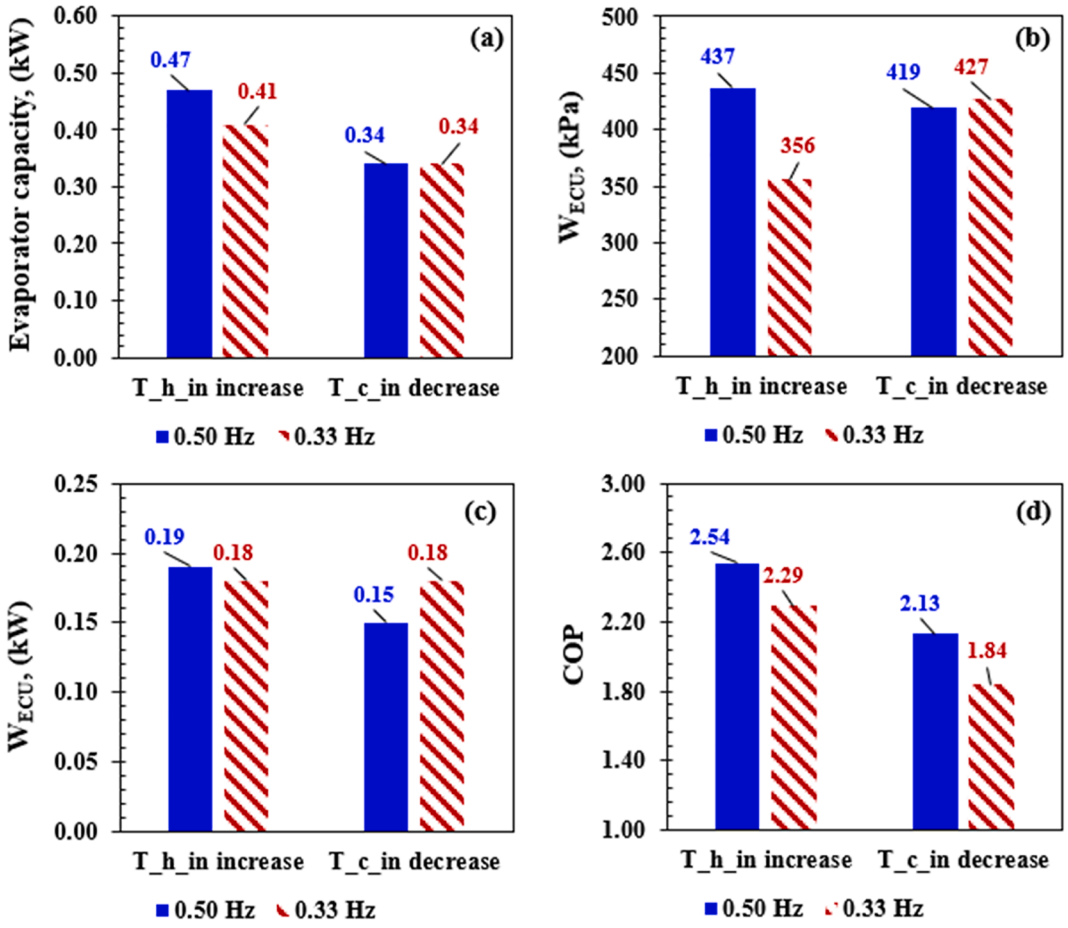

Fig. 18. Average performance indicators of the ECU-based system with the increase of the hot water temperature and the decrease of the cold water at 0.50 Hz and 0.33 Hz.

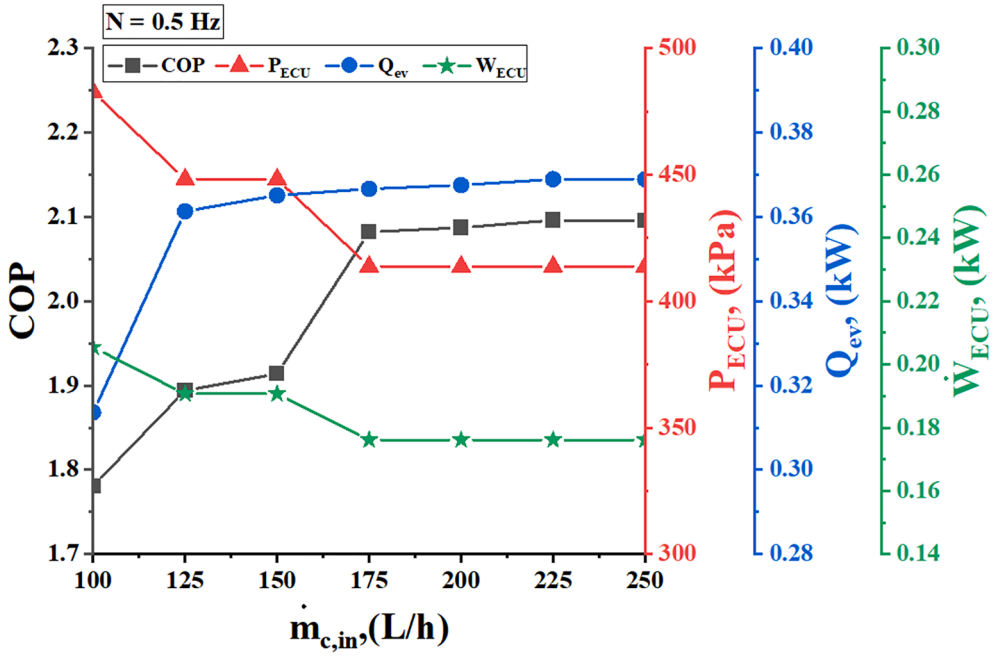

Fig. 19. Variation of the performance indicators with the cold-water flow rate at 0.5 Hz.

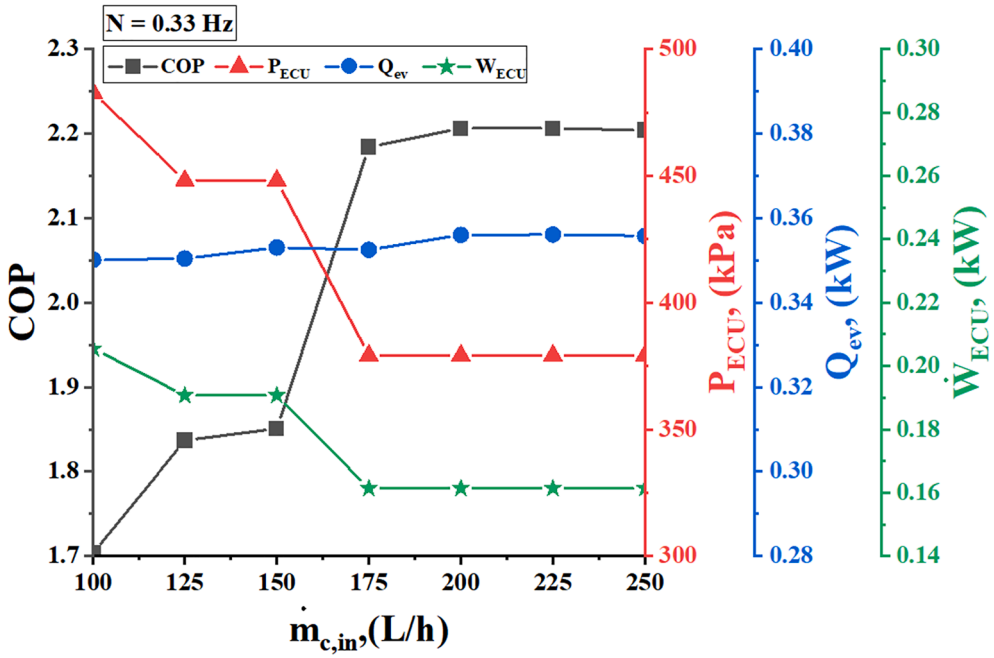

Fig. 20. Variation of the performance indicators with the cold-water flow rate at 0.33 Hz.

Table 7
Comparison between the characteristics, advantages, and limitations of the present ECU-based TMR system and ejector-based and ORC-based systems.

TMR technology	Heat source temp., (°C)	COP	Advantages	Limitations
ORC	100–300	0.10–0.75	Mature technology	Not economical at temperatures lower than 100 °C, moving parts
Ejector	85–160	0.10–0.62	Simple, low cost	Not flexible, not stable
ECU-based TMR	70–100	1.50–2.60	Simple, flexible capacity	Moving parts

- Over a wide range of testing conditions, the average COP of the ECU-based refrigeration system varies from 1.57 to 2.73 at frequency of 0.50 Hz from 1.56 to 2.39 at frequency of 0.33 Hz.
- The COP of the ECU-based refrigeration system is three times higher than the ejector-based systems and 2.70 times higher than the ORC-based systems.

Finally, the present experimental work proves the features of the ECU-based refrigeration at a wide range of testing conditions. Also, the obtained results can serve as a reference for further improved ECU design.

CRediT authorship contribution statement

Ahmad K. Sleiti: Conceptualization, Investigation, Writing – original draft, Writing – review & editing, Resources, Formal analysis, Project administration, Funding acquisition, Supervision. **Wahib A. Al-Ammari:** Conceptualization, Writing – original draft, Investigation, Software, Data curation, Validation, Formal analysis. **Mohammed Al-Khawaja:** Conceptualization, Project administration, Funding acquisition, Supervision. **Ahmad T. Saker:** Data curation, Validation.

Declaration of Competing Interest

The authors declare that they have no known competing financial interests or personal relationships that could have appeared to influence the work reported in this paper.

Acknowledgement

The work presented in this publication was made possible by NPRP-S grant # [11S-1231-170155] from the Qatar National Research Fund (a member of Qatar Foundation). The findings herein reflect the work, and are solely the responsibility, of the authors.

The authors acknowledge the efforts of Mr. Maxim Glushenkov and Mr. Alexander Kronberg in designing the expander compressor unit as part of their tasks in NPRP-S grant # [11S-1231-170155].

Appendix A:. Overall heat transfer coefficient between the brazed plate heat exchanger (BPHX) fluids and ambient air

Referring to Fig. A1 (c), the effective heat transfer area of a plate is given as [33]:

$$A_P = \Phi \bullet L_P \bullet W_P \tag{A.1}$$

where A_P, Φ, L_P, and W_P are the effective heat transfer area, enlargement factor, length, and width of the plate. The enlargement factor of the plate is the ratio between the plate effective heat transfer area (A_P), and the designed area ($W_P \times L_P$), and lies between 1.15 and 1.25. The plate length and width, also expressed in terms of port diameter (D_P), vertical port (L_V), and horizontal port distances (L_H) (see Fig. A1 (c)), as in Eqns. (2) and (3), respectively [33].

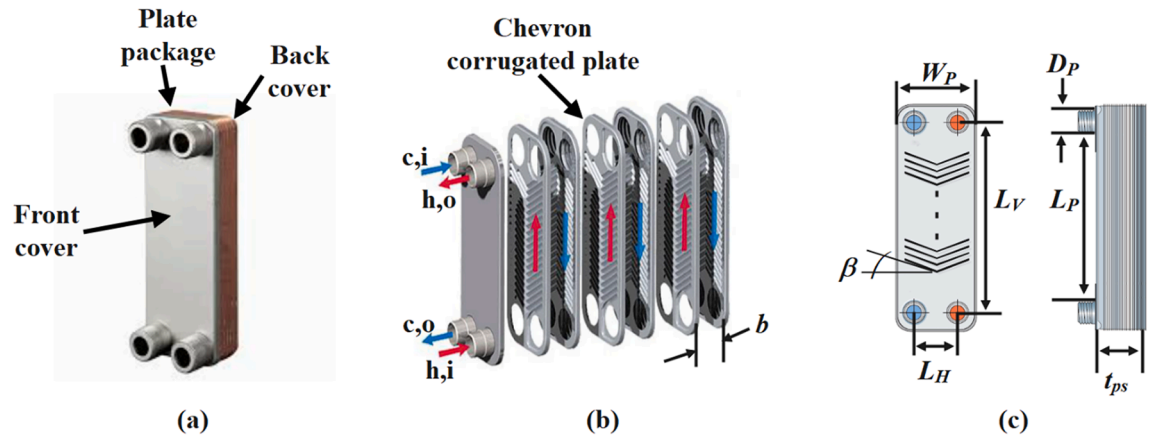

Fig. A1. Configuration of the brazed plate heat exchanger (BPHX): (a) isometric view, (b) expanded view, and (c) characteristic dimensions of a single-pass BPHX.

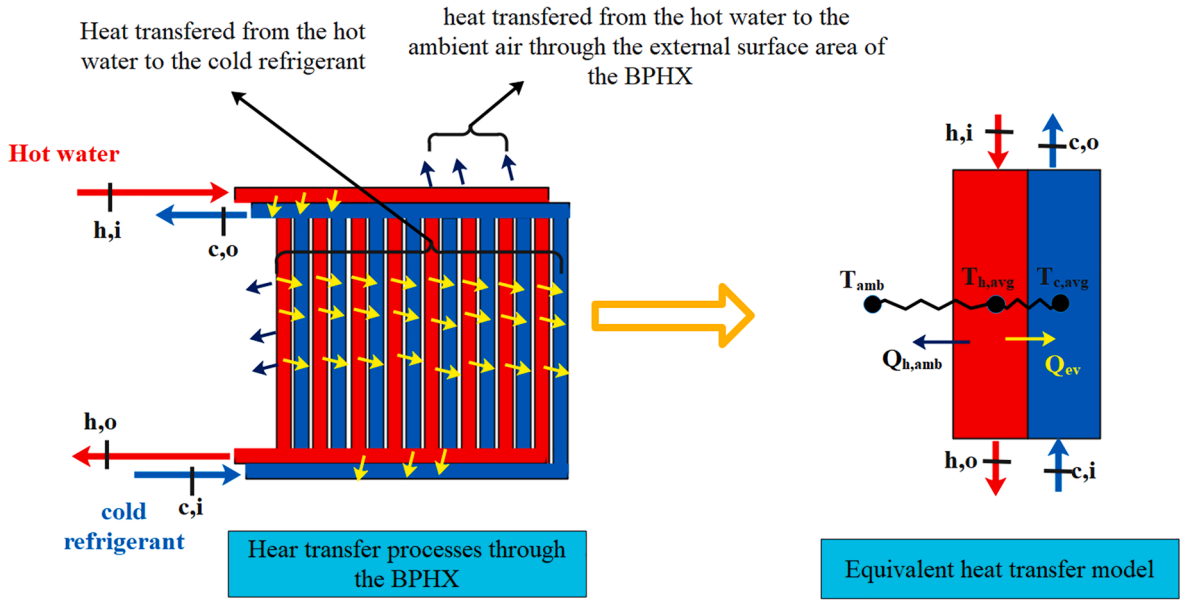

Fig. A2. Heat transfer process between the hot water and cold refrigerant and ambient in the evaporator of the cooling loop.

$$L_P \approx L_V - D_P \tag{A.2}$$

$$W_P \approx L_H + D_P \tag{A.3}$$

For the effective *heat* transfer area, the hydraulic diameter of the channel is given by the equivalent diameter (D_e) which is given as [33]:

$D_e \approx 2b/\Phi$(A.4) where b is the average thickness of the channel. The heat transfer rate between the hot fluid at the end plates of the BPHX and the ambient (see Fig. A2.) air is expressed based on the mass flow rate and enthalpies of the hot fluid (or cold fluid) as:

$$Q = \dot{m}_h(h_{h,i} - h_{h,o})/N_{plates} \tag{A.5}$$

Also, the heat transfer rate is expressed in terms of the global design equation:

$$Q = U \bullet A \bullet (T_{h,avg} - T_{amb}) \tag{A.6}$$

where U is the overall heat transfer coefficient with the ambient, and A is the total surface area of heat exchanger. The overall heat transfer coefficient is given as:

$$U = \frac{1}{\frac{1}{h_h} + \frac{1}{h_{air}} + \frac{t_P}{k_P} + R_{f,h}} \tag{A.7}$$

where h_h is the heat transfer coefficients of the hot fluid, and h_{air} is the free (or forced) the heat transfer coefficients of the ambient air. t_P and k_P are thickness and thermal conductivity of the plate.

$R_{f,h}$ and $R_{f,c}$ are the fouling factors of the hot and cold streams, respectively. The total heat transfer area (according to Fig. A.1) is given as:

$$A = 2 \times A_P + 2 \times t_{ps} \times L_V + 2 \times t_{ps} \times W_P \tag{A.8}$$

For the calculations of the heat transfer coefficients of the hot fluid, the Reynolds number (Re) and Nusselt number are given as:

$$Re = \frac{G_C D_e}{\mu} \tag{A.9}$$

$$G_C = \frac{\dot{m}}{N \bullet b \bullet W_P} \tag{A.10}$$

$$Nu = C_h Re^n Pr^{1/3} \left(\frac{\mu}{\mu_w}\right)^{0.17} \tag{A.11}$$

where G_C is the mass flow rate per channel, μ is the dynamic viscosity of the fluid (taken at the average temperature of the inlet and outlet temperatures), N is the channel number per pass,C_h and n are constants given as a function of Re and β (chevron corrugation inclination angle). Pr is Prandtl number, μ_w is viscosity at the wall temperature. Once the Nusselt number is obtained, the heat transfer coefficient of each stream is obtained from:

$$Nu = \frac{h \bullet D_e}{k} \tag{A.12}$$

For the free heat transfer coefficient of the ambient air (h_{air}), it is given as [34]:

$$h_{air} = k_{air} Nu_{air} / W_P \tag{A.13}$$

where k_{air} is the thermal conductivity of the ambient air and W_P is considered here as the characteristic length of the hot surface. The Nusselt number of the ambient air (for free convection) is given as [34]:

$$Nu_{air} = \frac{g \bullet \beta \bullet (T_{s,BPHX} - T_{air}) \bullet W_P^3}{\nu_{air} \bullet \alpha_{air}} \tag{A.14}$$

where g, β, $T_{s,BPHX}$, ν_{air}, and α_{air} are the gravitational acceleration, coefficient of volume expansion, surface temperature of the BPHX, kinematic viscosity of the air, and the thermal diffusivity of the air, respectively. The surface temperature of the BPHX is taken as the average between the hot fluid temperature and ambient air temperature.

References

[1] International Energy Agency (IEA). The Future of Cooling: Opportunities for energy- efficient air conditioning. 2018.

[2] L.L. Jia, R. Zhang, X. Zhang, Z.X. Ma, F.G. Liu, Experimental analysis of a novel gas-engine-driven heat pump (GEHP) system for combined cooling and hot-water supply, Int. J. Refrig. 118 (2020) 84–92, https://doi.org/10.1016/j.ijrefrig.2020.04.033.

[3] Y. Li, R.Z. Wang, Photovoltaic-powered solar cooling systems, Adv. Sol. Heat. Cool. (2016), https://doi.org/10.1016/B978-0-08-100301-5.00010-2.

[4] R.M. Lazzarin, Solar cooling: PV or thermal? a thermodynamic and economical analysis, Int. J. Refrig. 39 (2014) 38–47, https://doi.org/10.1016/j.ijrefrig.2013.05.012.

[5] I. Sarbu, C. Sebarchievici, General review of solar-powered closed sorption refrigeration systems, Energy Convers. Manag. 105 (2015) 403–422, https://doi.org/10.1016/j.enconman.2015.07.084.

[6] M. Zeyghami, D.Y. Goswami, E. Stefanakos, A review of solar thermo-mechanical refrigeration and cooling methods, Renew. Sustain. Energy Rev 51 (2015) 1428–1445, https://doi.org/10.1016/j.rser.2015.07.011.

[7] K. Bataineh, Y. Taamneh, Review and recent improvements of solar sorption cooling systems, Energy Build. 128 (2016) 22–37, https://doi.org/10.1016/j.enbuild.2016.06.075.

[8] A.B. Little, S. Garimella, A critical review linking ejector flow phenomena with component- and system-level performance, Int. J. Refrig. 70 (2016) 243–268, https://doi.org/10.1016/j.ijrefrig.2016.05.015.

[9] X. Chen, S. Omer, M. Worall, S. Riffat, Recent developments in ejector refrigeration technologies, Renew. Sustain. Energy Rev. 19 (2013) 629–651, https://doi.org/10.1016/j.rser.2012.11.028.

[10] B. Xu, D. Rathod, A. Yebi, Z. Filipi, S. Onori, M. Hoffman, A comprehensive review of organic rankine cycle waste heat recovery systems in heavy-duty diesel engine applications, Renew. Sustain. Energy Rev. 107 (2019) 145–170, https://doi.org/10.1016/j.rser.2019.03.012.

[11] A. Auld, A. Berson, S. Hogg, Organic rankine cycles in waste heat recovery: a comparative study, Int. J. Low-Carbon Technol. 8 (suppl 1) (2013) i9–i18, https://doi.org/10.1093/ijlct/ctt033.

[12] A.K.A.K. Sleiti, W.A. Al-Ammari, M. Al-Khawaja, W.A. Al-Ammari, M. Al-Khawaja, Review of innovative approaches of thermo-mechanical refrigeration systems using low grade heat, Int. J. Energy Res. 44 (2020) 9808–9838, https://doi.org/10.1002/er.5556.

[13] K. Rahbar, S. Mahmoud, R.K. Al-Dadah, N. Moazami, S.A. Mirhadizadeh, Review of organic Rankine cycle for small-scale applications, Energy Convers. Manag. (2017) 135–155, https://doi.org/10.1016/j.enconman.2016.12.023.

[14] A. Mahmoudi, M. Fazli, M.R. Morad, A recent review of waste heat recovery by Organic Rankine Cycle, Appl. Therm. Eng. 143 (2018) 660–675, https://doi.org/10.1016/j.applthermaleng.2018.07.136.

[15] B.M. Tashtoush, M.A. Al-Nimr, M.A. Khasawneh, A comprehensive review of ejector design, performance, and applications, Appl. Energy 240 (2019) 138–172, https://doi.org/10.1016/j.apenergy.2019.01.185.

[16] A.K. Sleiti, W.A. Al-Ammaria, M. Al-Khawaja, A novel solar integrated distillation and cooling system - design and analysis, Sol. Energy 206 (2020) 68–83, https://doi.org/10.1016/j.solener.2020.05.107.

[17] M. Glushenkov, A. Kronberg, T. Knoke, E. Kenig, Isobaric expansion engines: new opportunities in energy conversion for heat engines, pumps and compressors, Energies 11 (1) (2018) 154.

[18] A.K. Sleiti, W.A. Al-Ammaria, M. Al-Khawaja, M. Karbon, W.A. Al-Ammari, A combined thermo-mechanical refrigeration system with isobaric expander-compressor unit powered by low grade heat – design and analysis, Int. J. Refrig. 120 (2020) 39–49, https://doi.org/10.1016/j.ijrefrig.2020.08.017.

[19] A.K. Sleiti, W.A. Al-Ammari, M. Al- Khawaja, W.A. Al-Ammaria, M. Al-Khawaja, Analysis of novel regenerative thermo-mechanical refrigeration system integrated with isobaric engine, J. Energy Resour. Technol. 143 (2021) 1–10, https://doi.org/10.1115/1.4049368.

[20] A.K. Sleiti, Isobaric expansion engines powered by low-grade heat—working fluid performance and selection database for power and thermomechanical refrigeration, Energy Technol. 8 (2020) 2000613, https://doi.org/10.1002/ente.202000613.

[21] M. Al-khawaja, A.K. Sleiti, W.A. Al-ammari, Geothermics energy conversion of heat from abandoned oil wells to mechanical refrigeration - transient analysis and optimization, Geothermics 97 (2021), 102269, https://doi.org/10.1016/j.geothermics.2021.102269.

[22] L. Jiang, H. Lu, R. Wang, L. Wang, L. Gong, Y. Lu, A.P. Roskilly, Investigation on an innovative cascading cycle for power and refrigeration cogeneration, Energy Convers. Manag. 145 (2017) 20–29, https://doi.org/10.1016/j.enconman.2017.04.086.

[23] N. Chaiyat, Y. Wakaiyang, X. Inthavideth, Enhancement efficiency of organic Rankine cycle by using sorption system, Appl. Therm. Eng. 122 (2017) 368–379, https://doi.org/10.1016/j.applthermaleng.2017.05.028.

[24] Y. Huang, P. Jiang, Y. Zhu, Experimental and modeling studies of thermally-driven subcritical and transcritical ejector refrigeration systems, Energy Convers. Manag. 224 (2020), 113361, https://doi.org/10.1016/j.enconman.2020.113361.

[25] X. Wang, Y. Zhang, Y. Tian, X. Li, S. Yao, Z. Wu, Experimental investigation of a double-slider adjustable ejector under off-design conditions, Appl. Therm. Eng. 196 (2021), 117343, https://doi.org/10.1016/j.applthermaleng.2021.117343.

[26] Y. Lu, T. Bai, J. Yu, Experimental investigation on a -40 °C low-temperature freezer using ejector-expansion refrigeration system, Int. J. Refrig. 118 (2020) 230–237, https://doi.org/10.1016/j.ijrefrig.2020.06.010.

[27] T. Bai, H. Xie, S. Liu, G. Yan, J. Yu, Experimental investigation on the influence of ejector geometry on the pull-down performance of an ejector-enhanced auto-cascade low-temperature freezer, Int. J. Refrig. 131 (2021) 41–50, https://doi.org/10.1016/j.ijrefrig.2021.08.021.

[28] Zhang K, Qu T, Zhou D, Jiang H, Lin Y, Li P, et al. Digital twin-based opti-state control method for a synchronized production operation system. Robot Comput Integr Manuf 2020;63:101892. https://doi.org/10.1016/j.rcim.2019.101892.
[29] S. Aphornratana, T. Sriveerakul, Analysis of a combined Rankine-vapour-compression refrigeration cycle, Energy Convers. Manag. 51 (2010) 2557–2564, https://doi.org/10.1016/j.enconman.2010.04.016.
[30] A.K. Sleiti, W.A. Al-ammari, Off-design performance analysis of combined CSP power and direct oxy-combustion supercritical carbon dioxide cycles, Renew. Energy 180 (2021) 14–29, https://doi.org/10.1016/j.renene.2021.08.047.
[31] Y. Yang, Y. Zhu, Z. Zhang, R. Li, Z. Sun, C. Huang, Experimental study on performance of double-mode refrigeration system, Appl. Therm. Eng. 188 (2021), 116670, https://doi.org/10.1016/j.applthermaleng.2021.116670.
[32] V. Nair, A.D. Parekh, P.R. Tailor, Experimental investigation of a vapour compression refrigeration system using R134a/Nano-oil mixture, Int. J. Refrig. 112 (2020) 21–36, https://doi.org/10.1016/j.ijrefrig.2019.12.009.
[33] F.A.S. Mota, E.P. Carvalho, M.A.S.S. Ravagnani, Modeling and design of plate heat exchanger, Heat Transf. Stud. Appl. (2015), https://doi.org/10.5772/60885.
[34] A. Cengel Y, J. Ghajar A. Heat and Mass Transfer, Fundamentals & Application, Fifth Edition in SI Units. 2015.